# Chapter 2
# Chip-Level Degradation of InGaN-Based Optoelectronic Devices

**Carlo De Santi, Matteo Meneghini, Gaudenzio Meneghesso, and Enrico Zanoni**

**Abstract** This chapter reviews the main physical mechanisms responsible for the degradation of InGaN-based optoelectronic devices at chip level. The generation of defects caused by bias and temperature is frequent in modern devices, being responsible for the increase in non-radiative recombination and forward leakage current. Deep level enhancement related to diffusion will also be discussed. The investigation will then move to further processes, such as degradation of the ohmic contacts, electromigration, and device cracking due to mismatch. In addition, we described failure processes related to extrinsic factors, namely, electrostatic discharges and electrical overstresses, along with possible structure improvements that permit to increase device robustness. Finally, degradation caused by reverse bias will be investigated, a topic of growing interest for the design of AC-powered LEDs.

## 2.1 Defect Generation

The presence of defects in the device is one of the main factors that limit the optical performance. Defects may be native, when they originate from undesired arrangements of the crystal lattice, or extrinsic, when they are related to external impurities. Common native defects include missing gallium or nitrogen atoms in an expected position, called vacancies ($V_{Ga}$, $V_N$), presence of gallium or nitrogen atoms in locations that are not part of the lattice (interstitials $Ga_i$, $N_i$), and gallium or nitrogen atoms occupying the site of their counterpart (substitutionals $Ga_N$, $N_{Ga}$). These may be point defects, when only one atom is involved, or arranged in 2D or 3D configurations, giving birth to extended defects and dislocations. Typical external contaminants include impurities, such as silicon and magnesium that are introduced in order to achieve n- and p-type conductivity, respectively. Other elements present in the growth reactor may have a negative impact, such as hydrogen from the precursors (known for its passivating effect on p-type doping [1, 2]) and residual

C. De Santi • M. Meneghini • G. Meneghesso • E. Zanoni (✉)
Department of Information Engineering, University of Padova, Padova, Italy
e-mail: enrico.zanoni@unipd.it



W.D. van Driel et al. (eds.), *Solid State Lighting Reliability Part 2*, Solid State Lighting Technology and Application Series 3, DOI 10.1007/978-3-319-58175-0_2

oxygen (which is probably involved in the strong yellow luminescence of GaN [3, 4]). Native and extrinsic defects may form bonds, creating several different kinds of complexes.

Defects can create allowed energy levels inside the forbidden bandgap, acting as non-radiative recombination centers according to the Shockley-Read-Hall (SRH) theory, and therefore they reduce the number of electron-hole pairs available for radiative recombination and emission of desired photons.

In a first-order approach, the overall efficiency of LEDs can be described by using the ABC model:

$$\eta_{\mathrm{EQE}} = \eta_{\mathrm{extr}} \times \eta_{\mathrm{inj}} \times \frac{\mathrm{B}n^2}{\mathrm{A}n + \mathrm{B}n^2 + \mathrm{C}n^3}$$

where $\eta_{EQE}$ is the external quantum efficiency, $\eta_{extr}$ the extraction efficiency, $\eta_{inj}$ the injection efficiency, A the Shockley-Read-Hall coefficient, B the radiative recombination coefficient, C the Auger recombination coefficient, and $n$ the carrier density. It is typically assumed that the radiative recombination coefficient does not change during stress, and experimental data obtained at low bias current have a negligible contribution from Auger recombination. At chip level, a variation in the extraction efficiency would require extensive modification in the device structure, since it is related to the reflectivity of the front and back surfaces. In summary, the analysis of the EQE at the various steps of the aging can provide useful information on the variation in SRH recombination and radiative efficiency. In the following, both processes will be analyzed.

### *2.1.1 Increase in Non-radiative Losses*

A comprehensive study identifying the increase in the SRH coefficient as the cause for the optical degradation and its effects was carried out by La Grassa et al. [5]. The devices under test are single quantum well (SQW) LEDs grown on a silicon substrate. Stress caused a reduction in the external quantum efficiency, as shown in Fig. 2.1a. The effect is stronger in the low-moderate current regime, suggesting an increase in the SRH coefficient. The same effect may also be explained by an enhanced carrier escape or shunt leakage current contribution; therefore an additional experiment was designed. By using a highly focused laser diode with adequate peak wavelength, electron-hole pairs were created only inside the quantum well, and the photoluminescence (PL) and corresponding photocurrent were monitored during aging. Results, reported in Fig. 2.1b, show that the PL decreases and that this effect cannot be explained by a higher carrier escape because the corresponding photocurrent, shown in the inset, decreases. The reduction in both quantities can be explained by the additional $e^-$–$h^+$ loss process induced by the higher SRH recombination.

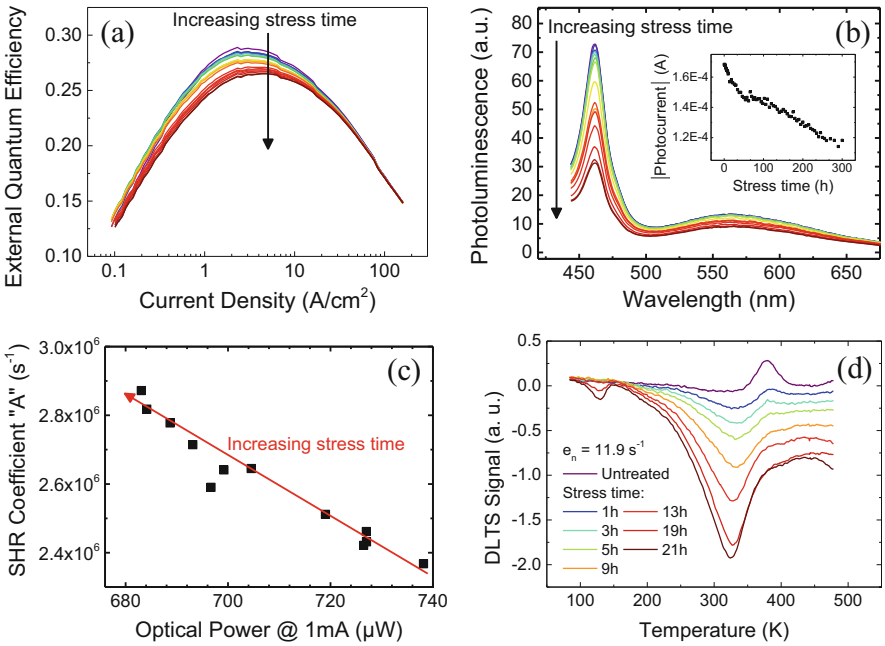


**Fig. 2.1** The reduction in optical power at low-medium bias current (**a**) in SQW LEDs is associated to a lower photoluminescence (**b**). This effect is not caused by a higher leakage from the quantum well since the corresponding photocurrent does not increase (inset), but by an enhanced SRH non-radiative recombination, well correlated to the variation in optical power (**c**). The stronger C-DLTS signal (**d**) confirms the increased defect density (Reprinted from Microelectronics Reliability, vol. 55, no. 9–10, M. La Grassa, M. Meneghini, C. De Santi, M. Mandurrino, M. Goano, F. Bertazzi, R. Zeisel, B. Galler, G. Meneghesso, E. Zanoni, "Ageing of InGaN-based LEDs: Effects on internal quantum efficiency and role of defects,", pp. 1775–1778, Copyright (2015), with permission from Elsevier.)

Direct measurement of the SRH A coefficient is possible, thanks to the differential carrier lifetime technique [6]. In this case, an enhancement in non-radiative (SRH) recombination was experimentally found, well correlated with the reduction in the output optical power, as reported in Fig. 2.1c. By means of capacitance deep level transient spectroscopy (C-DLTS, [7]), an increase in defect density for a deep level located at $E_c$–0.61 eV was detected (see Fig. 2.1d), confirming that the measured increase in non-radiative recombination is supported by physical modification in the lattice and not caused by additional effects or measurement artifacts.

### *2.1.2 Increase in Shunt Current*

Tracking changes in the injection efficiency is not an easy task, since there is no clear way to distinguish electron-hole pairs lost due to shunt conduction paths or to

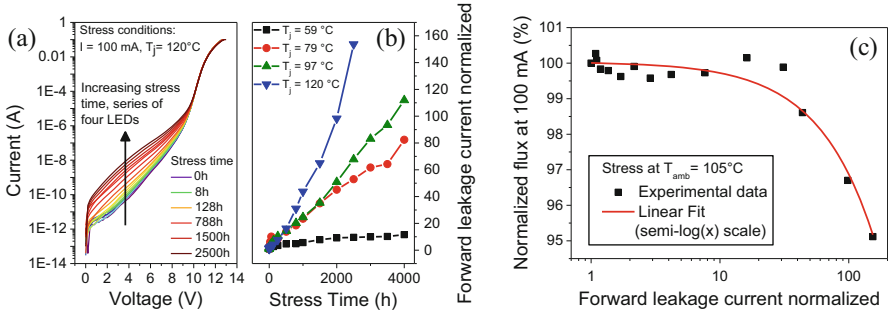


**Fig. 2.2** (**a**) Aging causes an increase of the forward leakage current in the series of four white LEDs, (**b**) enhanced by the junction temperature during the stress at the same bias current. (**c**) The variation is well correlated with the decrease in output optical power (Reprinted from Microelectronics Reliability, vol. 55, no. 9–10, M. Buffolo, C. De Santi, M. Meneghini, D. Rigon, G. Meneghesso, E. Zanoni, "Long-term degradation mechanisms of mid-power LEDs for lighting applications", pp. 1754–1758, Copyright (2015), with permission from Elsevier.)

non-radiative recombination in the quantum well. A study involving the possible role of the forward leakage in the degradation of LEDs was presented by Buffolo et al. [8]. They tested the reliability of medium-power white LEDs stressed at nominal operating current and various junction temperatures, evaluated according to the forward-voltage technique [9].

Figure 2.2a reports the changes induced by the stress in the current-voltage characteristics of four LEDs connected in series configuration. A strong increase in the forward leakage current below 10 V is clearly visible, and its amount is influenced by the junction temperature during the stress (see Fig. 2.2b). Recent works correlate the current at low forward bias with the trap-assisted tunneling through mid-gap defects located in the quantum wells, the spacer, and the electron-blocking layer [10, 11]. Therefore, the experimental data are consistent with the creation of deep levels inside the device enhanced by the temperature. The increase in forward leakage is well correlated with the reduction in the output optical power, as described in Fig. 2.2c, possibly because the defect-related conductive path shunts the quantum wells, preventing part of the radiative recombination and lowering the injection efficiency. It is important to point out that, since the defects responsible for the increased forward leakage are located also in the quantum wells, it is possible that the lower optical flux is partly caused by the higher SRH recombination at this new defect and not only by the reduced injection efficiency.

## 2.2 Diffusion Processes

The defects responsible for the higher SRH recombination may be generated locally by the combined effect of current and temperature, or they can be originated by the diffusion of preexisting defects or impurities towards the active region.

In the literature, several models are available for describing the time dependence of the diffusion process. One of the most successful is the solution in one dimension of Fick's second law, as described by Orita et al. [12]. Assuming a constant $N_0$ concentration of impurities diffusing toward the active region, the amount of impurities $N_{\text{diff}}$ at the position $x$ after time t can be described as

$$N_{\text{diff}}(x,t) = N_0 \ \text{erfc}\left(\frac{x}{2\sqrt{\text{Dt}}}\right)$$

where D is the diffusion coefficient and erfc the error function. According to the SRH theory, a higher local defect concentration yields a faster recombination through deep levels and therefore a lower non-radiative lifetime $\tau_{nr}$. Its variation therefore follows the equation:

$$\Delta\left(\frac{1}{\tau_{\text{nr}}}\right) = \frac{\text{KN}_0}{w}\int_0^w \text{erfc}\left(\frac{x}{2\sqrt{\text{Dt}}}\right)\text{dx}$$

where K is a coefficient that is related to carrier capture rate and $w$ the width of the space charge region.

Diffusion is easier to detect in laser diodes (LD), owing to the linear relation between reciprocal carrier lifetime and threshold current $I_{th}$

$$I_{\text{th}} = \frac{\text{qV}}{\eta_{\text{inj}}}\frac{N_{\text{th}}}{\tau_{\text{nr}}}$$

where $q$ is the absolute value of the electron electrical charge, V the volume of the active region, and $N_{th}$ the carrier density at lasing threshold. Therefore, if a diffusion process is responsible for the degradation of a laser diode, the expected variation of the threshold current should follow a $\sqrt{t}$ dependence on stress time.

This model was successfully used by De Santi et al. to describe the threshold current variation in commercial green InGaN-based laser diodes submitted to accelerated lifetime tests [13]. The good fitting quality (not shown here) suggested the presence of a diffusion process, and in order to gain additional information, the authors carried out high-resolution spectrally resolved cathodoluminescence maps on the samples. This technique allows for selective excitation of electron-hole pairs in a limited volume of the device by means of a high-energy electron beam. The full emission spectrum is then recorded point by point and analyzed to detect the local composition and radiative efficiency.

Figure 2.3a shows the results at the front facet of an untreated LD. Each color represents the intensity recorded at a specific wavelength (emitted by a specific layer); color coding was done as described in Fig. 2.3b. The saturation level of the color is proportional to the CL signal intensity, i.e., a brighter color points out regions with high radiative efficiency and low defect-related non-radiative recombination. It can be clearly seen that the optical performances of the device are

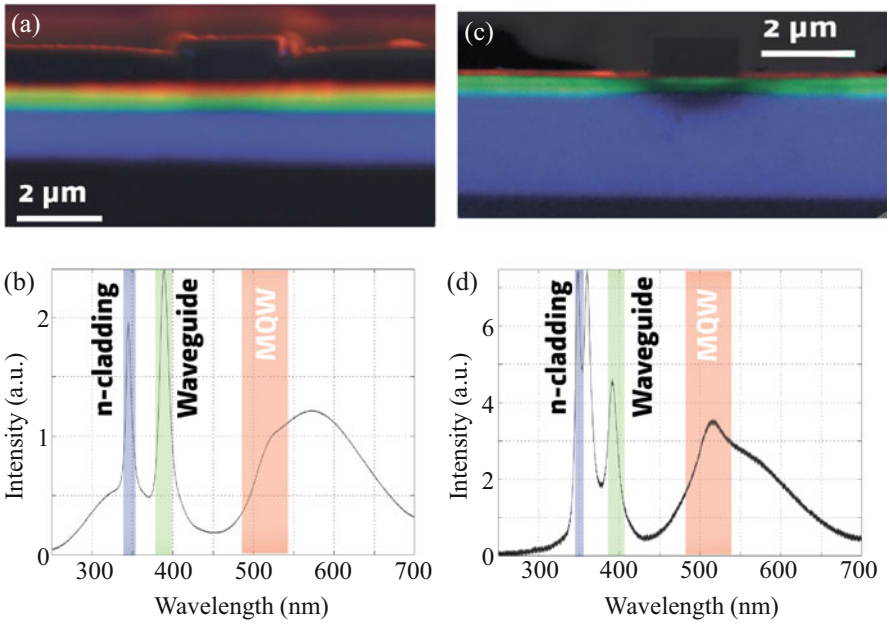


**Fig. 2.3** Comparison between high-resolution cathodoluminescence maps at the front facet of an (**a**) untreated and (**c**) aged laser diode. The spectra integrated over the whole area, along with the explanation of the color coding, are shown in (**b**) and (**d**), respectively (Reprinted from De Santi et al. [13]. © 2016 IEEE)

uniform over the whole area under investigation. The intensity profile completely changes when a stressed device is tested (Fig. 2.3c, d). In this case, a dark zone identifies a local enhancement of the non-radiative recombination, affecting not only the quantum wells but also the waveguiding and cladding layers. It is worth noticing that the shape of the degraded region is semicircular and symmetrical along the axis from the p-side to the n-side (i.e., the direction of the current flow). This profile is compatible with a diffusion-related degradation originated from the p-side and moving toward the n-side. Possible culprits include magnesium and hydrogen, chemical elements present in the p-doped material in dopant-level concentration in a highly mobile interstitial position.

Additional information can be extracted by means of this innovative technique regarding the role of the yellow luminescence (YL) in the degradation of the device. The yellow luminescence is a parasitic radiative recombination path, involving gallium vacancies [14] and possibly enhanced by carbon [15–17] or oxygen [3, 4, 18]. In some cases the degradation of LEDs is associated to an increase in the yellow emission, and it is typically assumed that the reduction in optical power is caused by the higher SRH recombination at the defects responsible for the YL. In the case of the laser diodes under analysis, a stronger emission in the yellow spectral region was detected, but this was not the reason for the threshold current

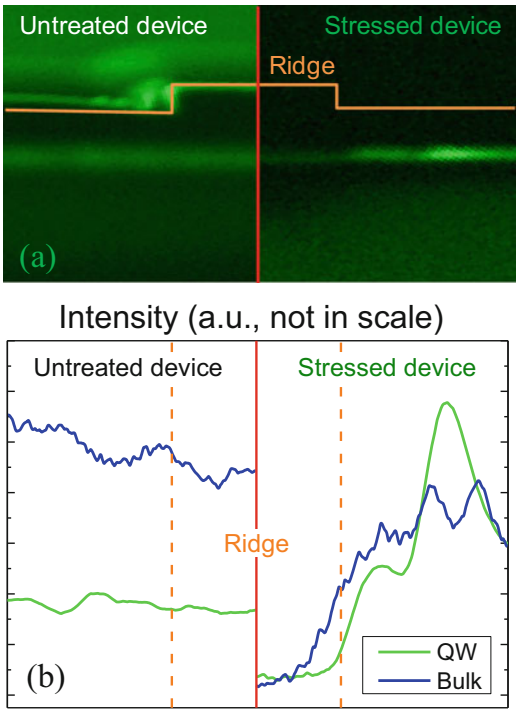


**Fig. 2.4** (**a**) Monochromatic cathodoluminescence maps highlighting the spatial distribution of the yellow luminescence in an untreated and stressed device. The latter is affected by the same non-radiative reduction already described for the band-to-band emission. (**b**) Reports the intensity profile along the quantum wells and the bulk material for clearer comparison (Reprinted from De Santi et al. [13]. © 2016 IEEE)

increase. As can be seen in Fig. 2.4a, even the YL signal is affected by an intensity reduction, with the same semicircular shape already described for the band-to-band luminescence. Figure 2.4b reports the intensity profiles in the quantum wells and in the bulk material, allowing for a better understanding of the different intensity. The experimental data are compatible with the generation of an additional deep level, draining electron-hole pairs both from the main emission and from the parasitic yellow band.

A more extensive set of reliability tests on the same samples was carried out by De Santi et al. in [19], varying both the junction temperature and the bias current in order to understand the role of the two stress stimuli. The threshold current was chosen as the parameter used to monitor the degradation.

Figure 2.5a reports its variation during aging at the same bias current and six different junction temperatures, evaluated by means of the forward-voltage method [9], along with a stress at the highest temperature and no applied bias. It can be noticed that no degradation occurs if no current flows through the device and that the degradation is thermally activated. The dashed lines are the fits according to the diffusion model described at the start of this section; the very good agreement suggests that the degradation can be caused by a diffusion process. From the fits it is possible to extrapolate the value of the diffusion coefficient, whose values are summarized in Fig. 2.5b. At higher temperatures the degradation is faster and therefore the diffusion coefficient is higher, and an activation energy of 1.98 eV

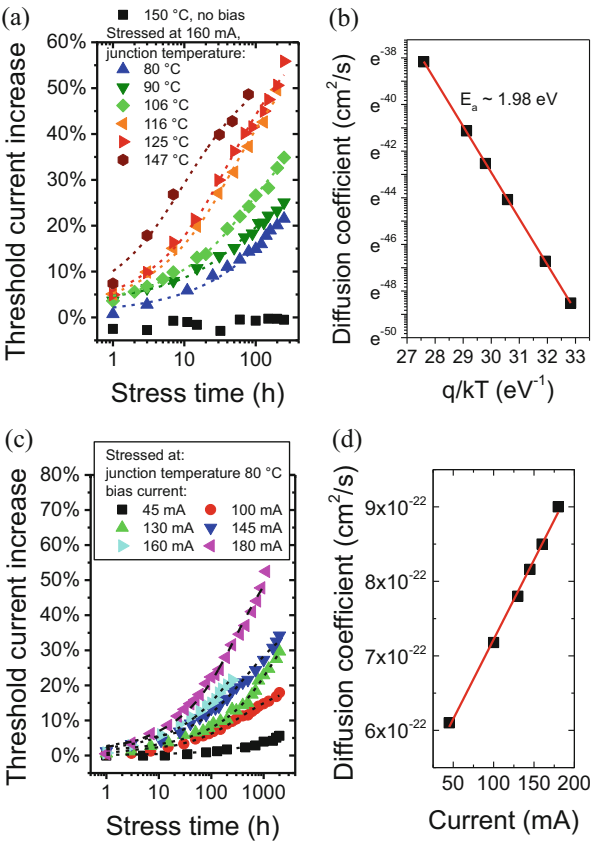


**Fig. 2.5** (**a**) Variation in the threshold current of green laser diodes stressed at different junction temperature and fit according to the diffusion equations; the extrapolated values of the diffusion coefficient and its activation energy are in (**b**). (**c**) Presents the same data for devices stressed at different bias currents, the diffusion coefficients are summarized in (**d**) (Reprinted from Microelectronics Reliability, vol. 64, C. De Santi, M. Meneghini, G. Meneghesso, E. Zanoni, "Degradation of InGaN laser diodes caused by temperature- and current-driven diffusion processes", pp. 623–626, Copyright (2016), with permission from Elsevier.)

can be calculated. This value is similar to the 1.93 eV found by Seager et al. in p-n junctions for hydrogen diffusion and even closer to the theoretical 2.03 eV for the sum of the activation energies for diffusion and binding of $H^+$ to Mg acceptors [20].

The results of the tests at different bias current are shown in Fig. 2.5c. Even in this case, the diffusion equations are able to closely model the experimental data. The diffusion coefficient values in Fig. 2.5d suggest that the bias current level has an impact, even though few reports are available concerning a possible drift mechanism during diffusion [20]. A complete explanation of the whole dataset requires careful examination of the possible diffusing species, their charge state, and their position in the lattice. Possible additional mechanisms that need to be taken into account include the dopant activation, the transfer of kinetic energy from the carriers to the diffusing elements, the field-assisted drift of the impurities, and the diffusion of native defects. Additional details are given in [19]. Moreover, recent papers propose that, during operation of a device, a possible release of hydrogen from point defects can take place, in particular from gallium vacancies [21, 22]. This process can lead to an increased local concentration of hydrogen over stress time. In summary, the data suggest that the degradation could be related to the

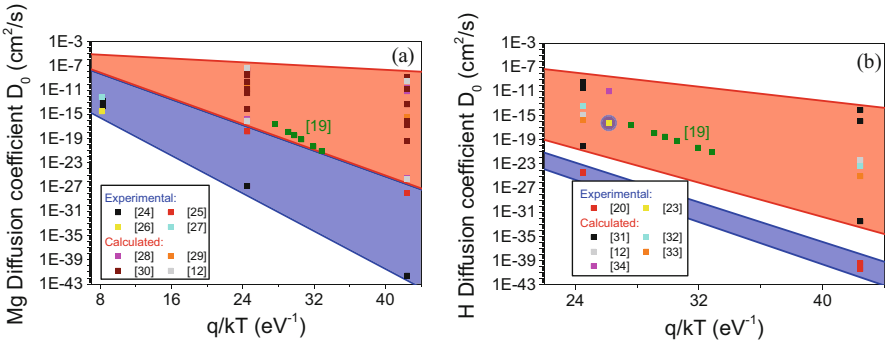


**Fig. 2.6** Experimental (*blue region*) and calculated (*red region*) diffusion coefficients for (**a**) magnesium and (**b**) hydrogen from the literature [12, 19, 20, 23–34] (Reprinted from Microelectronics Reliability, vol. 64, C. De Santi, M. Meneghini, G. Meneghesso, E. Zanoni, "Degradation of InGaN laser diodes caused by temperature- and current-driven diffusion processes", pp. 623–626, Copyright (2016), with permission from Elsevier.)

diffusion of interstitial $H^+$ from the p-side toward the n-side. It is enhanced by temperature, as any diffusion process, and by current, due to the lower electric field in the space charge region that opposes the diffusion.

The analysis of the bias role in the diffusion process has important consequences for a correct understanding of the mechanism. Figure 2.6a, b reviews experimental and theoretical diffusion coefficients reported in the literature for Mg and H, respectively. A clear difference between experimental values and parameters computed from first principles can be noticed. This broad variation may point out that the theoretical basis of the diffusion mechanism for these impurities is not yet completely understood and that the electric field may be a likely candidate to include in the calculations.

## 2.3 Degradation of the Ohmic Contacts

The ohmic contacts are critical regions, since they strongly influence the injection efficiency of the devices. The metal-semiconductor interface may be affected by interdiffusion, and in GaN the lack of metals with high work function requires very high doping levels for obtaining a tunneling Schottky junction at the p-side. Even though as-grown devices usually suffer from no contact-related performance reduction, additional problems may appear during the lifetime of the device.

A degradation mechanism present in early LEDs is the partial or total detachment of the Ti-W contact and reflector layer from the n-side of the device, reported by Meneghini et al. [35]. Reliability tests carried out in DC and pulsed condition showed that it causes an increase in the series resistance of the device.

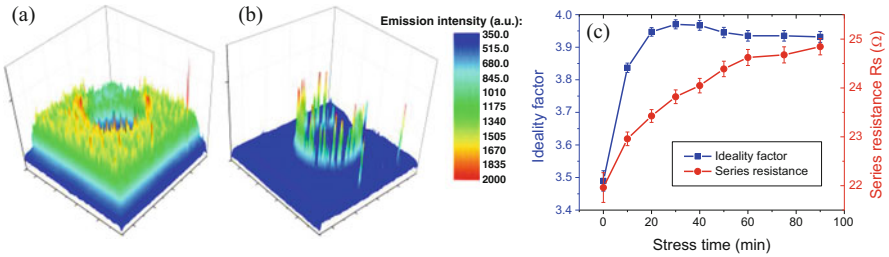


**Fig. 2.7** Spatial distribution of the electroluminescence in a LED (**a**) before and (**b**) after thermal storage at 250 °C and no applied bias, showing significant current crowding. The increase in series resistance caused by the aging is shown in (**c**)

In addition to macroscopic mechanical damage, degradation may occur due to microscopic changes in the semiconductor, more common in the latest generations due to the improvements in contact deposition technology. The first demonstration of a degradation mechanism related to this problem was given by Meneghini et al. [36]. They submitted two series of multiple quantum well (MQW) LEDs grown on SiC substrate to accelerated lifetime tests at temperatures between 180 and 250 °C with no applied bias. The devices differ in the presence or lack of SiN passivation deposited by plasma-enhanced chemical vapor deposition (PECVD). They found a strong decrease in optical power only in passivated devices, along with a significant variation in the spatial distribution of the electroluminescence. Figure 2.7 shows that the luminescence, compared to the untreated device (a), is clearly localized near the bonding pad in a device aged for 90 min (b). The current crowding yields also a remarkable increase in the overall series resistance of the device (see Fig. 2.7c). The suggested degradation mechanism involves the transfer of hydrogen from the passivation (the SiN precursors in PECVD are $SiH_4$ and $NH_3$) to the p-GaN layer. The H atoms may bond with magnesium, reducing the effective doping level and therefore increasing the resistivity of the contact. This supports the strong current crowding under the bonding pad, since the metal prevents H diffusion from the passivation to the semiconductor.

These tests do not identify whether the contamination problem affects only the contact or also the p-GaN contact layer. In order to clarify this point, additional tests were carried out by Meneghini et al. by using the transmission line method (TLM) [37]. Circular TLM patterns passivated by H-rich PECVD with different radii were submitted to thermal storage at 250 °C. As shown in Fig. 2.8a, the stress caused an increase in series resistance, as previously reported, but also a rectifying behavior near 0 V. This last effect may be related to the Mg deactivation due to H diffusion from the passivation. A lower effective doping level causes a broadening of the Schottky barrier between the metal and the semiconductor, lowering the tunneling probability of the electrons and therefore moving the contact from an ohmic to a rectifying behavior. The TLM technique allows for estimate of both contact and sheet resistance, whose changes over stress are reported in Fig. 2.8b. The increase in contact resistivity is stronger compared to sheet resistance, proving that degradation

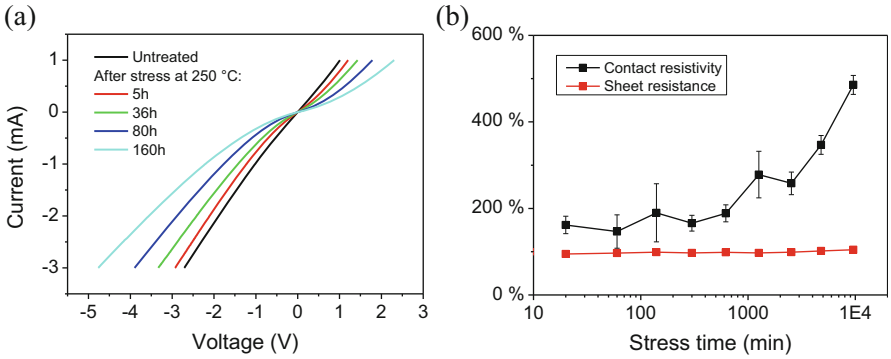


**Fig. 2.8** (**a**) Change from ohmic to rectifying behavior of the TLM structure during stress at 250 °C and (**b**) comparison between the variation of the contact and sheet resistance

mainly affects the semiconductor in close proximity to the passivation but not the whole p-GaN layer. In this case, the degradation was found to be recoverable. Additional thermal storage after device depassivation was able to partly restore the initial characteristics, likely due to hydrogen outgassing from the surface. The use of low-H sputtered SiN (instead of PECVD deposition) was able to lower the amount of degradation.

The deposition method for the passivation is not the only parameter influencing the reliability of the contacts. The metal stack composition has a strong importance, due to the very high interdiffusion coefficient of Ni and Au (reported in the 400–600 °C range in [38]). A detailed study on the stability of conventional Ni/Au contacts and on the use of $TiB_2$ or Ir as an interdiffusion barrier in MQW LEDs was given by Stafford et al. [39]. They found that a strong increase in the turn-on voltage could be caused by thermal storage at the relatively low temperature of 200 °C. The leakage current and output optical power were negatively affected by the test. An improvement of the long-term stability was obtained through the use of $TiB_2$/Ti/Au or Ir/Au overlayers between the Ni/Au contact and the p-GaN.

## 2.4 Electromigration

Electromigration is the movement of atoms from the contact pads or the current spreading metal lines to the semiconductor. This process is aided by the current flow, due to the energy exchange between the electrons and the metal atoms, and by the temperature, since it follows the laws of diffusion.

Electromigration has detrimental effects for the reliability of the device: the movement of the metal causes a variation in the local resistance, leading to current crowding. The higher current density induces a stronger local self-heating, and the increased temperature reduces the resistance even more. If this positive feedback is

too strong, it may cause the device to fail due to thermal runaway. In addition, if there is a preferential path for electromigration, a continuous metal line could form from the p-side to the n-side, effectively shunting the active region and preventing correct device operation.

Barton et al. showed that strong electrical degradation, up to a short-circuit behavior, may be present in blue GaN-on-sapphire LEDs [40, 41]. The devices under test were submitted to short (100 ns) but intense current pulses, and no significant change in capacitance DLTS signal was detected. Electron beam-induced current (EBIC) imaging highlighted the presence of some small conductive paths shunting the active region, and scanning electron microscope (SEM) secondary images revealed damage to the p-side contact compatible with metal migration. An electromigration process was therefore identified as the mechanism responsible for the degradation.

Kim et al. analyzed multi-quantum well InGaN/GaN LEDs grown on a sapphire substrate, carrying out stress tests at different bias levels on unpackaged samples [42]. They found that the lifetime can be explained by the contact electromigration failure model of silicon devices, and the increase in forward and reverse current was consistent with the role of metal electromigration in the degradation. Optical photographs of the pad surface support this hypothesis.

Both papers suggested a correlation between the amount of electromigration and defect density in the lattice, since dislocations are believed to be preferential paths for the migration of the metal atoms. Decisive evidence was provided in the study by Hsu et al. who analyzed the effect of high temperature annealing in GaN-on-sapphire MQW LEDs with Ni/Au contact layer [43]. Devices were tested at different annealing temperatures, from 300 to 900 °C, and each annealing test lasted for 10 min in a furnace with continuous nitrogen flow. They found an increase of the forward and reverse leakage currents even at the lower temperatures and a clear short-circuit behavior at higher temperatures. The morphology of the electrodes changed during the test due to the creation of some bubbles on the surface, and in order to investigate the cause, they carried out a transmission electron microscope (TEM) investigation of the cross section directly below the bubbles. The result is summarized in Fig. 2.9. Figure 2.9a shows, for the LED annealed at 900 °C, a hollow region at the center of the bubble in the metal contact directly above a dislocation in the lattice, whereas in Fig. 2.9b, a dislocation in the LED annealed at 600 °C. The labels highlight the points where energy-dispersive X-ray spectroscopy (EDX) was carried out in order to investigate the chemical composition. As can be seen, the void in the bubble (EDS-1) contains some gallium, probably originated by Ga outdiffusion, and the corresponding gasification of nitrogen during GaN decomposition could be the cause for the formation of the bubbles. The most important finding comes from the comparison of EDS-2 and EDS-3. Along the dislocation it is possible to find contamination of nickel and gold, but the two elements are not present outside the dislocation in the p-GaN layer. This experiment confirms that metal from the contacts can be prone to electromigration, that dislocation are preferential paths, and that this mechanism could cause

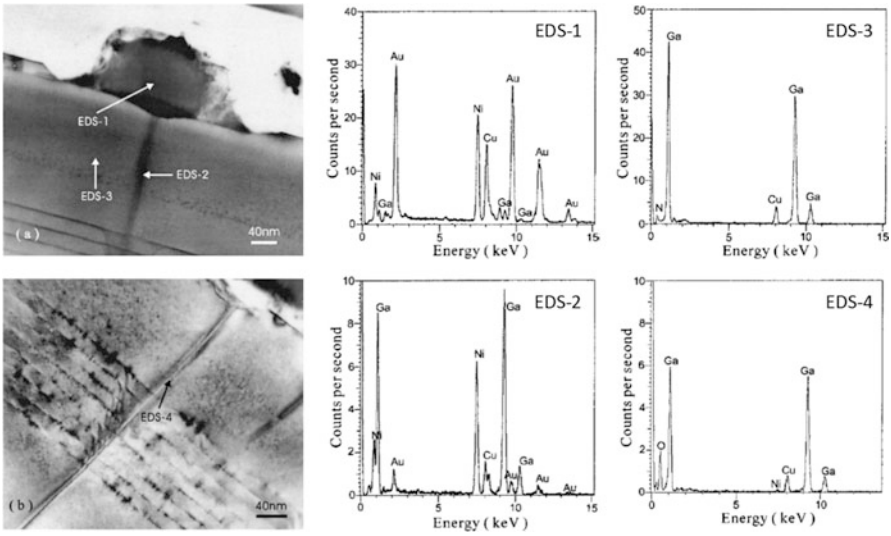


**Fig. 2.9** Cross-sectional TEM image of an LED annealed at (**a**) 900 °C and (**b**) 600 °C. EDX spectra (EDS from one to four) confirm the presence of metal atoms from the contacts only inside the dislocations, as a consequence of electromigration (Reproduced from Hsu, Chin-Yuan and Lan, Wen-How and Wu, YewChung Sermon, Applied Physics Letters, 83, 2447–2449 (2003), with the permission of AIP Publishing [43])

shunting of the device. Metal atoms are present also in the dislocations of device annealed at a lower temperature, even if in lower concentration (EDS-4).

Liu et al. in a recent work suggested that electromigration and mechanical stresses can cause a broadening of the contact metal lines [44]. They suppose that dislocation-related failure may happen even without metal atoms migrating inside the dislocation, due to the de-trapping of space charges around threading dislocations caused by the higher electric field at the rough metal edges. Additional work is required in order to confirm this hypothesis.

## 2.5 Cracking Due to Mismatch

Gallium nitride substrates would be the best choice for device growth, but the technical difficulties involved in the creation of large area native substrates are not easy to overcome. Available GaN wafers have a small area and a remarkable cost, causing a high price for the final products. For this reason, sapphire substrates are commonly used, and a lot of effort is put into growth of efficient LEDs on cheaper silicon substrates.

Both sapphire and silicon have high thermal expansion coefficient and lattice constants mismatch with gallium nitride. For this reason, a high density of

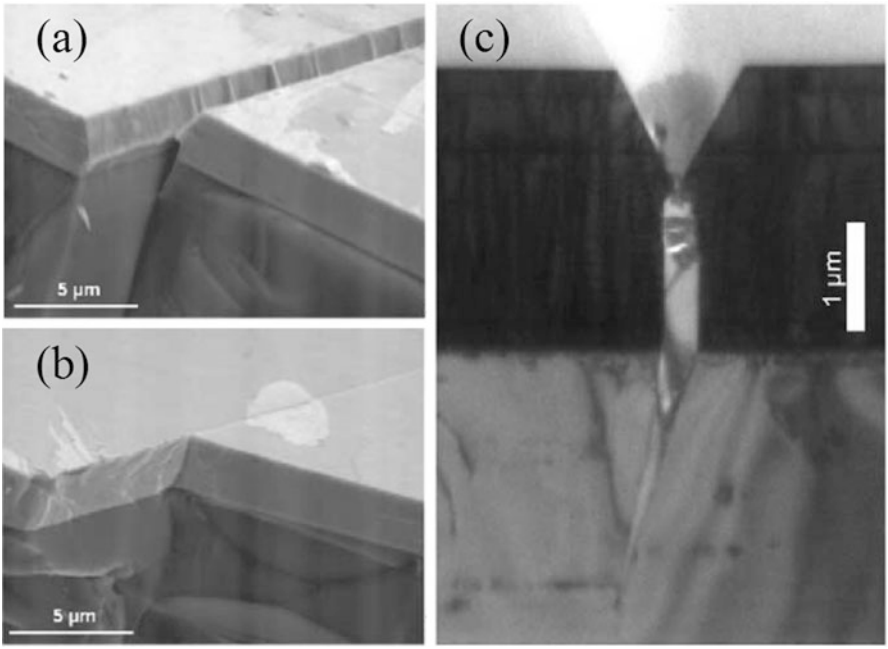


**Fig. 2.10** Possible types of cracks for GaN on Si: (**a**) open groove with facets (occurs during heating); (**b**) closed crack (occurs during cooling). The cross section of an open crack is shown in (**c**) (Reprinted from Materials Science and Engineering: B, vol. 93, no. 1-3, A. Krost, A. Dadgar, "GaN-based optoelectronics on silicon substrates", pp. 77–84, Copyright (2002), with permission from Elsevier.)

dislocations forms at the interface between the substrate and the epitaxial layer, reducing the efficiency and the reliability of the devices. Moreover, the strain may relax through the creation of extended cracks during growth or device operation. For GaN on Si, two different types of cracks can be found: open grooves with facets occurring during growth (see Fig. 2.10a) and a crack without grooves, likely generated during the cooling process (see Fig. 2.10b). The cracks extend into the silicon substrate (see Fig. 2.10c).

The formation of cracks in both heating and cooling stages was confirmed by Sarua et al. even for $Al_{0.34}Ga_{0.66}N$ layers grown on GaN on sapphire [46]. By means of atomic force microscope (AFM), they detected the formation of cracks after sample cooling from growth temperature to room temperature and the creation of additional but smaller cracks after annealing above 900 °C. The variation of the position of the $E_2$(high) phonon mode measured by Raman scattering confirms that tensile stress is relieved near the cracks and that annealing reduces the overall stress, thanks to the formation of the additional cracks (and to the possible formation of dislocations).

Barton et al. studied the degradation of several GaN LEDs grown on sapphire substrate [47]. They used electron beam-induced voltage (EBIV) mapping to

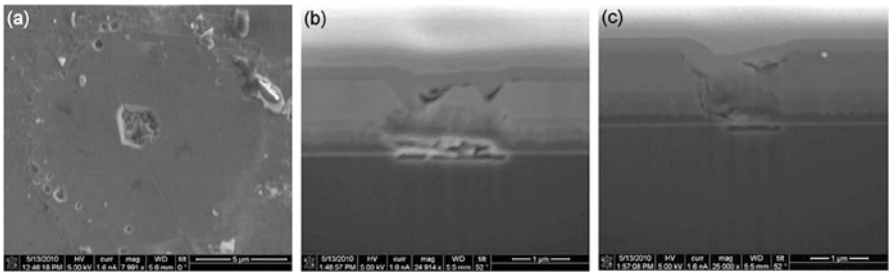


**Fig. 2.11** SEM images of a microvoid (**a**) at the center of the plane view, (**b**) and (**c**) at a FIB cross section (Reproduced from Blake, Adam H. and Caselli, Derek and Durot, Christopher and Mueller, Jason and Parra, Eduardo and Gilgen, Joseph and Boley, Allison and Smith, David J. and Tsong, Ignatius S. T. and Roberts, John C. and Piner, Edwin and Linthicum, Kevin and Cook, James W. and Koleske, Daniel D. and Crawford, Mary H. and Fischer, Arthur J., Journal of Applied Physics, 111, 033107 (2012), with the permission of AIP Publishing [70])

correlate a sudden decrease in optical power with the formation of a crack in the device, isolating part of the active region from the contacts.

Various solutions are proposed in the literature to minimize the effects of mismatch, such as AlAs buffer layers [48, 49], AlN buffer layers [50–52], low-temperature AlN interlayers [53–55], AlGaN buffer layers [56], graded AlGaN buffer layers [57–59], superlattices [60–62], use of SiN interlayer [63], growth on patterned substrates [64–66], and growth on porous Si [67–69].

More recently, Blake et al. grew MQW InGaN/GaN LEDs on silicon substrate. The strain was relieved by means of $ZrB_2$ buffer layers and by an AlN/AlGaN/GaN transition layer [70]. Lateral cracks originated by microvoids were found on the surface of the LEDs (see in Fig. 2.11a a SEM image of a microvoid), completely quenching the electroluminescence from a vast area of the device. By means of cross-sectional transmission electron microscopy (XTEM) investigation, they showed that the presence of microvoids is not related to micropipes originating from the $ZrB_2$ buffer layer. A SEM analysis of a vertical focused ion beam (FIB) cross section revealed, under the microvoids, the presence of vertical cracks originating from thicker $ZrB_2$ regions, likely due to misoriented crystallites in the epitaxial $ZrB_2$ layer. Figure 2.11b, c is SEM cross sections of the region under the microvoid at two different steps of the FIB milling, showing cracks originating from distinctive features at the substrate interface. Devices without $ZrB_2$ buffer were not affected by this problem.

## 2.6 Electrostatic Discharge (ESD)

All electronic devices in every material system have a limited robustness to short and highly energetic stimuli, including GaN-based light-emitting diodes. These electrostatic discharge events (ESD) may last for a few hundreds of nanoseconds

and are originated from interaction with electrostatically charged manufacturing or handling equipment (machine model, MM), with installers or end users (human-body model, HBM), with ambient conditions in a typical operating environment (e.g., lightning for streetlight lamps), or with grounding connections when some residual charge is present on the device (charged-device model, CDM).

### *2.6.1 Role of Defects and Internal Capacitance*

Critical regions for the reliability are defective parts and unwanted leakage paths, where the high energy of the discharge may cause a significant current to flow. Typical weak regions are the edges of the contact layer [71–73], the edge of the bonding pad [74, 75], and V-pits with threading dislocations [75, 76]. For this reason, LEDs are sensitive to ESD of both negative and positive polarity, even though the latter usually causes less damage, thanks to the ability of the diode to sustain very high forward currents for a short amount of time before thermal damage occurs [73, 75].

Two different parameters seem to play an important role in the failure mechanism of an LED submitted to electrostatic discharges: the presence of V-pits with threading dislocations and the overall internal capacitance of the device.

The first step in identifying the importance of V-shaped defects connected to threading dislocations was reported by Su et al. [75]. They designed InGaN/GaN MQW LEDs on a sapphire substrate with a Mg-doped GaN cap layer grown at two different temperatures, low temperature grown (LTG) at 900 °C and 1,000 °C, and high temperature grown (HTG) at 1,040 °C and 1,100 °C. The surface of the HTG devices was very smooth with almost no visible extended defects, whereas the LTG devices showed a very rough surface due to the presence of a high V-pit density. The difference was ascribed to the low migration speed of Ga atoms at lower temperatures, leading to a low lateral growth rate [77–79]. Even though all the LEDs showed similar robustness to positive polarity ESD, HTG devices were able to withstand an almost double voltage during negative discharges.

This work was further expanded by Tsai et al. [76]. They grew InGaN/GaN MQW LEDs on a sapphire substrate with different p-GaN growth conditions. A first set of samples, labeled LED-II, used a layer with low temperature grown at 850 °C, leading to a high concentration of V-pits connected to threading dislocations (see a SEM top-view image and a TEM cross section in Fig. 2.12a). In the second set of samples, LED-III, the Mg-doped layer, was grown in HTG conditions at 1,050 °C, preventing the formation of V-pits consistently with the previous paper but not affecting significantly the threading dislocation density (see Fig. 2.12b). The last set of samples, LED-I, was designed with a hybrid approach: a HTG layer is grown immediately above the quantum wells, followed by a LTG layer. This way, the surface of the sample is even rougher than LED-II due to the high concentration of V-pits, but the bottom of the pit is not connected to a threading dislocation, whose density was not reduced (see Fig. 2.12c). Figure 2.12d reports the results of the ESD

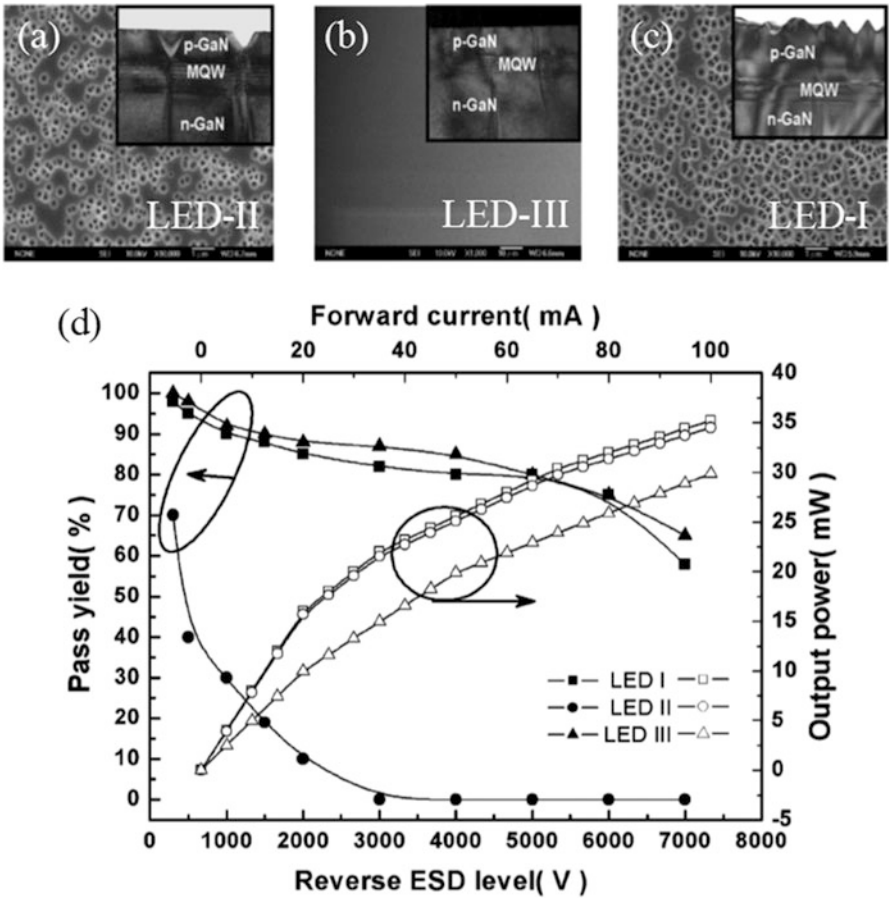


**Fig. 2.12** SEM top-view image and TEM cross section of MQW LEDs with p-GaN layer (**a**) grown at 850 °C, (**b**) grown at 1,050 °C, and (**c**) composed of two subsequent layers grown at 1,050 °C and 850 °C. The ESD robustness and output optical power for the different growth conditions are reported in (**d**) (Reprinted from [76]. © 2016 IEEE)

tests. Devices with basic structure (LED-II) have a limited robustness, whereas HTG devices (LED-III) have a higher reliability, consistent with the paper by Su et al. [75]. Remarkably, LED-I samples have a pass yield comparable to LED-III devices, due to the suppression of threading dislocations connected to V-pits. Compared to LED-III set, LED-I devices have a higher output optical power, related to the better extraction efficiency at the rough surface.

Concerning the internal capacitance, its importance derives directly from general considerations on energy transfer during the discharge. Each ESD event is based on a rapid charge transfer, which is simulated through the charge and discharge of an external capacitance on the device under test. In this case, the average current I flowing through the LED is given by $I = Q/\tau$, where $Q$ is the total

charge stored in the discharging capacitance $C_d$ and $\tau$ the time constant of the discharge process, which in a simple RC circuit is given by $\tau = C_i(R_{LED} + R_{\text{par}})$, where $C_i$ and $R_{\text{LED}}$ are the parallel capacitance and the parallel resistance of the device under test, respectively, and $R_{\text{par}}$ the parasitic resistances in the discharge circuit. When the LED resistance dominates in the time constant equation, the energy dissipation $E_d$ in the LED can be evaluated as $E_d = R_{\text{LED}} I^2 \tau = Q^2/C_i$ [80]. For this reason, the higher the capacitance of the LED, the lower energy dissipation it has to sustain. This basic reasoning was experimentally confirmed by Jeon et al. [81]. They grew InGaN MQW LEDs on sapphire substrate with different Si doping concentration in the n-side. The higher doping level increases the capacitance of the device under reverse-bias condition, i.e., when the border of the space charge region is located deep in the doped contact layer. They detected a higher robustness for more highly doped devices.

A similar experiment was carried out by Jia et al. [82]. They grew three different sets of InGaN MQW LEDs on sapphire substrate. Set A has a common structure, whereas set B has a 15 nm thick Si-doped (carrier concentration $1.5 \times 10^{19}$ cm$^{-3}$) InGaN layer between the bulk n-GaN and the MQWs. Additionally, set C has also a three-period modulation-doped p-InGaN/GaN hole injection layer between the p-GaN contact layer and the MQWs, where the GaN layers are unintentionally p-doped. The n-InGaN layer caused a small increase of the device capacitance, whereas a stronger effect was detected for devices with the p-superlattice. The ESD performances were improved by the higher internal capacitance.

A multilayer approach was exploited also by Li et al. at the n-side of InGaN MQW LEDs on sapphire substrate [80]. In this case, the improved devices possess three n-GaN/u-GaN pairs between the n-spacer layer and the active region. Experimentally, this additional insertion layer increased the capacitance of the device in the reverse-bias region and the ESD robustness.

### 2.6.2 ESD Effects

In order to understand the role of process and internal parameters in determining the ESD robustness, the simple pass-fail tests used in the previously reported papers are adequate. With the aim of explaining the effects of a discharge and the changes leading to the failure, more accurate and diverse tests are required.

SEM mapping of the samples is a good complementary technique, allowing for microscopic analysis of the differences between working and failed samples and for detection of most likely failure regions. This technique was used by Meneghini et al. during the tests of UV LEDs (see Fig. 2.13) [73]. The analysis of failed devices pointed out that the failure was located in a curved region of the contacts, where the mesa edge was irregular. This could lead to higher local electrical field and therefore to lower ESD robustness. As a consequence of the discharge, the region is affected by significant structural damage, preventing proper operation of the device.

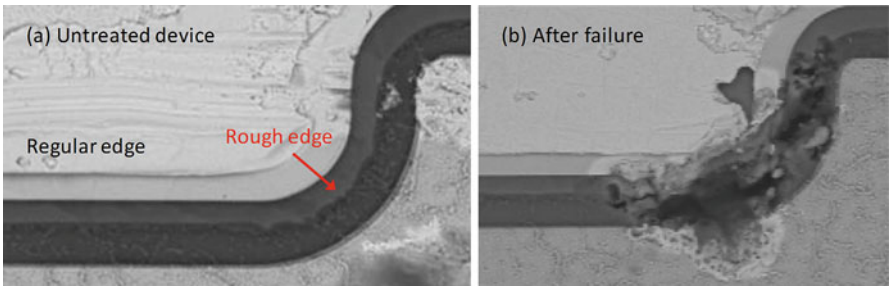


**Fig. 2.13** SEM images of an (**a**) untreated and (**b**) failed device submitted to ESD discharges. The correlation between irregular borders of the mesa and failed regions can be noticed

An additional technique that can be used in order to understand the effect of the ESD events is the emission microscopy. The spatially resolved electroluminescence in reverse-bias condition, along with the reverse leakage, was monitored by Meneghini et al. during ESD events at increasing voltage simulated by a transmission line pulser (TLP) on green LEDs [83]. They found that, after the first discharges up to −60 V, the characteristics of the device remained stable. Any additional discharge then reduced the leakage current and emission intensity, until the strong increase in leakage and drop in EL associated to the catastrophic failure of the device. The spatial distribution of the reverse luminescence showed that the reduction is related to the disappearance of some of the "hot spots" composing the emission. The lower leakage current can therefore be associated to local destruction of conductive paths, rather than to processes affecting a wide area. This annihilation may be related to the high energy associated to the pulses, and therefore it is consistently present only when the voltage is higher than a threshold value. When the energy is too high, the conductive paths may melt leading to a short circuit rather than to a nonconducting behavior.

Emission microscopy can be used to detect and support the analysis of different failure modes caused by ESD discharges in devices with varying structure and indium content in the quantum wells, as reported by Dal Lago et al. [84]. They tested two different series of commercially available LEDs, blue with a grid-shaped metal contact and green with a simple bonding pad, monitoring the change in the device impedance and electroluminescence during the discharge. The failure of blue LEDs was identified by the instantaneous increase in the leakage current, related to the creation of a low-resistance conductive path caused by the high power dissipated during the ESD event. This conductive path can be detected by the increase in luminescence after the catastrophic breakdown, occurred at $V_{LINE} = 1{,}503$ V in the case of the representative sample of Figs. 2.14a and 2.15. Subsequent discharges cause a sudden decrease in the impedance of the device, highlighted by the increase in the current flowing through the device during the ESD pulse in Fig. 2.14a. The emitting area moves toward the edge of the damaged region after every additional event (see Fig. 2.15), suggesting a diffusion of the conductive path and more significant damage in the central region, where current

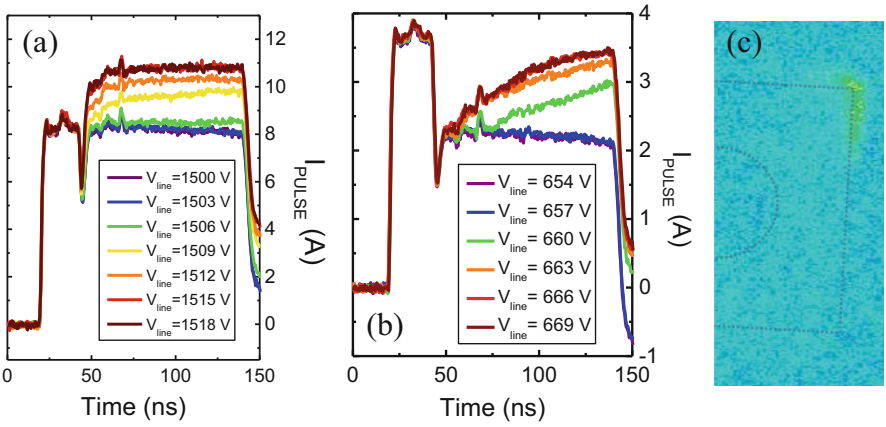


**Fig. 2.14** Results of ESD tests on commercial *blue* (**a**) and *green* (**b**), (**c**) LEDs. (**a**, **b**) Current flowing through the device during the discharge, highlighting variation in the device impedance; **c** electroluminescence during the pulse, showing the location of the damaged area (Reprinted from Microelectronics Reliability, vol. 53, no. 9-11, M. Dal Lago, M. Meneghini, N. Trivellin, G. Mura, M. Vanzi, G. Meneghesso, E. Zanoni, ""Hot-plugging" of LED modules: Electrical characterization and device degradation", pp. 1524–1528, Copyright (2013), with permission from Elsevier.)

flows no more. After the test, the device appears melted in the region corresponding to the emitting area. Concerning green LEDs, the increase in leakage current is gradual, and modifications in the device impedance take place even during the pulse, as can be noticed by comparing Fig. 2.14a, b, representative of blue and green devices, respectively. In this case, the emission during the discharge comes from the edge of the device (see Fig. 2.14c), suggesting that an improvement in the defect concentration along the device perimeter could lead to a significantly enhanced ESD robustness.

### *2.6.3 Structure Improvements*

Several solutions for improving the ESD robustness are available at device level and at circuit level. This chapter is focused on the reliability at chip level; therefore we will present only changes to the internal device structure and not designs requiring external components. For this reason, every possible design variation may cause also a positive or negative effect on the output optical power of the LED, other than an improvement of ESD robustness.

Chen et al. suggested a selective post-epitaxy etching and re-deposition in order to fabricate on-chip antiparallel GaN Schottky diodes [85]. Even if the etched areas were placed under the pads (to prevent loss of useful emitting area), in this case the emission from the protected LEDs was lower. The cause was ascribed to the increased non-radiative recombination at the defects generated by the etching process.

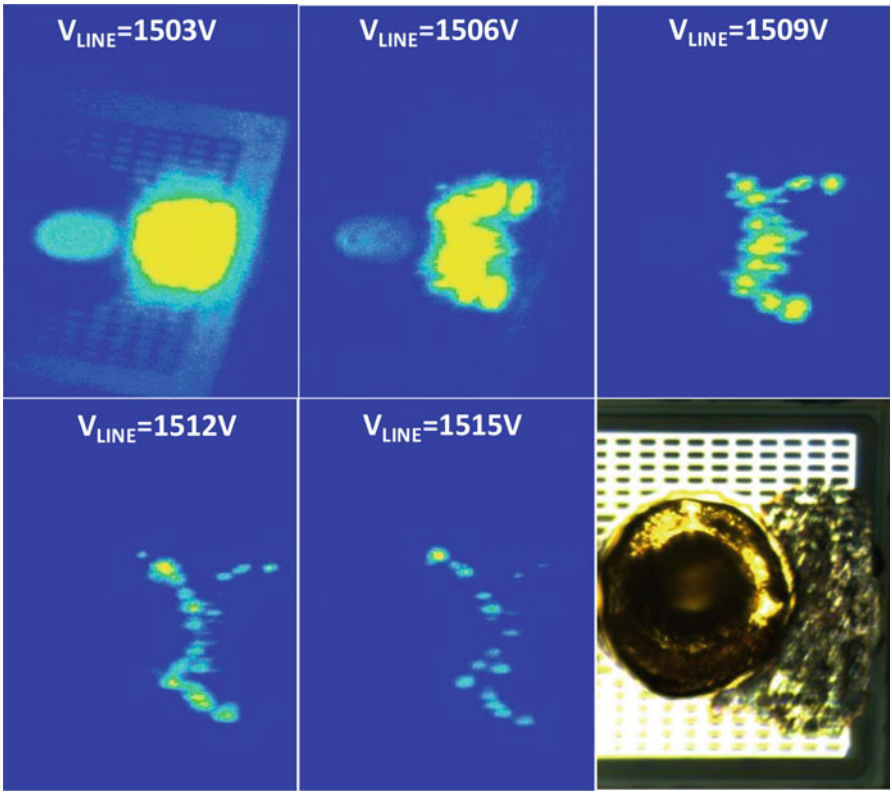


**Fig. 2.15** Electroluminescence during the ESD test on the commercial *blue* LED of Fig. 2.14**a**, showing the location and time evolution of the damaged area. The last frame (*bottom right*) shows a photo of the failed device

Wen et al. used an $Al_{0.12}Ga_{0.88}N$/GaN superlattices for a better spreading of the ESD-related current [86]. The superlattices were placed between the active region and the Si-doped GaN substrate (on the n-side) or the Mg-doped GaN cap (on the p-side). They were modulation doped (Si or Mg) to reduce their resistivity, leading to a significant increase of the robustness under reverse-bias pulses. No variation was detected with forward bias tests. The superlattice approach was used also by Liu et al. [87]. In this case the superlattice was composed of p-GaN/i-InGaN layers placed between the multiple quantum wells and the p-GaN layer. The output optical power of the device with superlattice was higher, due to a more uniform current spreading and to a possible reduction in injection losses.

The higher robustness to positive polarity discharges of the GaN-based LEDs was exploited by Shei et al. [88] and by Jeong et al. [89]. By using a selective etching, they realized two independent LEDs with different area on the same epitaxial wafer. The LEDs were then connected in antiparallel configuration by the metal lines, allowing the lower area device to act as an internal shunt protection

diode. In this case, the output optical power is lowered, since part of the area is used for the protection structure.

Following the previously described approach by Tsai et al. [76], Jang et al. studied the effect of the p-AlGaN EBL thickness. They found an improvement of the ESD robustness when a thicker EBL is present in the structure, assuming that it may be related to the filling of the dislocation-related v-pits [90]. The corresponding increase in electroluminescence was related to the lower carrier losses due to overflow and/or tunneling mechanisms.

A creative solution was suggested by Park et al. [91]. They added an air gap in an Al film below the substrate, connecting one side to the anode and the other one to the cathode. If the width of the gap is correctly designed, when the bias pulse is applied, current flows not through the LEDs but through the air gap, due to the limited dielectric strength of air. For this reason, this structure is able to protect the device from both negative- and positive-polarity discharges. No indication was given on the effect of the air gap on the optical characteristics.

Tsai et al. manufactured an internal MOS capacitor by adding a $SiO_2$ layer in the n-GaN epilayer and extending the metal lines from the contacts [92]. They tested several line layouts and found that the capacitor increases the robustness of the device. Subsequent discharges may lead to damage and puncturing of the oxide and in some cases even damage to the device occurs. The authors do not report the variation of the optical power in the different structures, but it is probably lower due to the area used up by the protection structure.

Chen et al. demonstrated, by means of 3D simulations and experimental tests, the importance of the metal line layout even when a MOS capacitor is not present [93]. They found that current density and thermal dissipation peaks may be reduced by a more uniform distribution of the electric field during the electrostatic discharge. The improved contact structure with parallel extended electrodes theoretically offers the best uniformity of the electric field and was experimentally demonstrated as the most reliable solution against both forward- and reverse-polarity discharges. Even in this case, no indication was given on the variation of the optical power when different contact geometries are employed.

A different solution was used by Huang et al., involving accurate design of a patterned substrate [94]. They tested several devices with different values of fill factor and slanted angle. LEDs grown on substrates with lower fill factor showed a lower concentration of threading dislocations and therefore higher reliability. The most robust devices also have higher output optical power, due to the lower threading dislocation density and to the higher light extraction efficiency.

More recently, Lee et al. suggested the possibility of realizing patterned damage in the current-blocking layer by means of oxygen plasma treatment ion damage [95]. The patterned ion-damaged current-blocking layer (IDCBL) increases the robustness of the devices due to the better spreading of the current injected by the ESD event. Devices with IDCBL were found to have a higher electroluminescence level, thanks to the improved current injection and current spreading, and possibly to a better extraction efficiency.

## 2.7 Electrical Overstress (EOS)

Compared to ESD events, even electrical overstresses (EOS) can induce catastrophic damage due to stimuli beyond the safe operating area, but involve longer (in the millisecond-second range) and less energetic stresses.

A possible cause is the connection of a LED to a power supply with enabled output, for example, when a lamp is plugged to an energized driver. This event, called "hot plugging," leads to a significant current flowing through the devices and to a possible degradation or failure. Dal Lago et al. carried out an extensive investigation of the mechanism and of its causes, testing several LEDs from various manufacturers, with varying peak wavelength, connected in series of different length, and even analyzing several drivers [96]. The current waveforms recorded during the hot plugging show that a significant overcurrent may flow through the devices and that its intensity is inversely proportional to the number of LEDs connected in series (see Fig. 2.16a). This behavior is consistent with the discharge of the output capacitance of the driver, charged up to the maximum allowed voltage value due to the lack of any load. This hypothesis was verified by simulation of the discharge time constant in a simple equivalent circuit composed of the output capacitance of the driver and a capacitance with a series resistance in order to

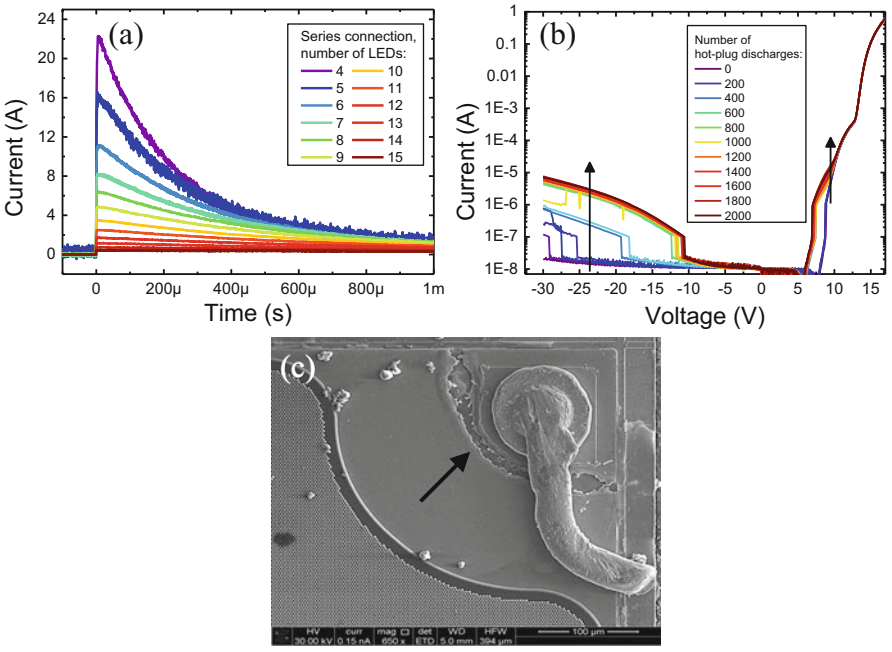


**Fig. 2.16** (**a**) Current waveforms during the "hot plugging" event as a function of the number of LEDs connected in series configuration. (**b**) Variation of the current-voltage characteristic after several "hot plugging" connections. (**c**) SEM image showing localized damage around the bonding pad

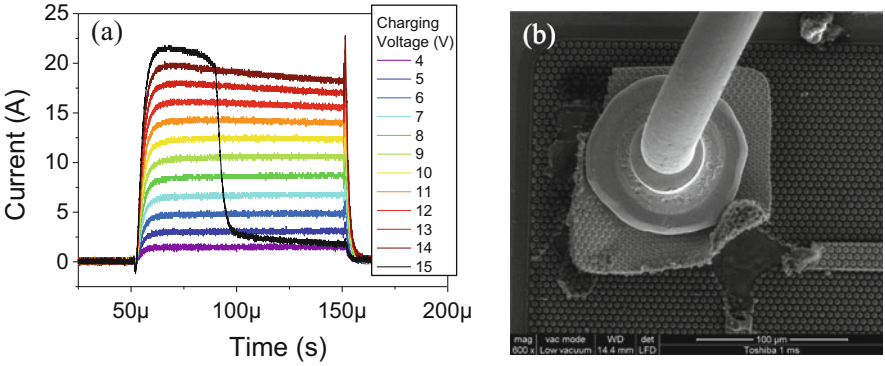


**Fig. 2.17** (**a**) Current waveforms during an EOS event at several voltages. (**b**) SEM image showing localized damage at the bonding pad and metal lines

model each LED. Repeated tests on the same LED series showed that the main effect of the event is the creation of defects inside the lattice, acting as additional paths for current flow and therefore increasing the forward and reverse leakage (see Fig. 2.16b). Inspection of failed samples reveals a preferential damaged area near the bonding pad (see Fig. 2.16c). The melted appearance suggests the important role of the device heating during the discharge, possibly due to current crowding leading to thermal runaway.

Additional tests were carried out by Meneghini et al. by using a custom EOS simulator in order to prevent effects related to the specific driver model and manufacturer [97]. Figure 2.17a reports typical current waveforms measured during an EOS event at several voltages. Failure is highlighted by a sudden decrease in the current flowing through the device. The increase in the impedance may be related to damage to the bonding pad and/or to the metal lines (see Fig. 2.17b). The amount of current required for the failure was found to be several times the nominal operating current and to strongly depend on the pulse width, confirming the important role of temperature and the current crowding hypothesis.

## 2.8 Reverse-Bias Degradation

In the past, reliability studies of LEDs in reverse-bias operation were of limited interest since LEDs are designed for forward bias operation, but this is going to change in the next years. Several research centers and companies are currently developing LED lamps able to operate when directly connected to the mains wall plug, i.e., in AC condition. These lamps do not require an external driver and converter, and therefore they have no additional size, weight, and reliability issue related to additional electronic components. Moreover, they have no power conversion losses and a reduced price due to the lower number of components and to the lower design cost. These advantages have a drawback related to the specific

LED configuration used in the lamps: the reverse-bias degradation issue. Typical AC lamp structures are composed of two LED stripes connected in antiparallel configuration (which improves also the robustness to ESD, since every stripe protects its neighbor). When the lamp is biased, one strip emits light during the positive half of the mains wave, the other during the negative [98–101]. The "off" stripe has to sustain the entire negative mains voltage, and process variations in the equivalent reverse resistance may lead to significant voltage dropping on a limited set of LEDs. For this reason, the analysis of the stability under strong reverse bias is important for this application [102–104].

Chen et al. tested the reliability of green InGaN/GaN MQW LEDs on sapphire substrate when submitted to reverse bias in water vapor [105]. They report a strong increase in the reverse current and in the forward bias leakage current, up to the failure of the device due to the formation of a short circuit. The degradation caused the decrease in the EL in specific regions of the device and the increase in the reverse-bias emission in the same locations. EDX analysis revealed the presence of Au from the contacts near the quantum wells, which may cause a peak in the local electric field. The authors conclude that the catastrophic failure occurs due to the high electric field, but since the stress tests were carried out in water vapor, it is not clear if the same degradation mechanism may influence AC lamps.

An extensive experiment was carried out in air by Meneghini et al. on green MQW LEDs stressed at several constant reverse current and reverse voltage values [106]. They provide experimental evidence that, in reverse-bias condition, current flows through preferential localized paths due to a tunneling process and is correlated to the reverse-bias luminescence. The reliability tests cause a strongly correlated increase in both current and EL, not related to the small power dissipation. The degradation rate was found to depend linearly on the stress current and almost exponentially on stress voltage, suggesting an important role of hot carriers. Stresses at varying temperature showed that the enhancement in degradation rate is stronger for constant voltage tests rather than constant current, confirming that carrier density is the driving force for the increase in reverse current. Failure is therefore related to the generation or propagation of defects toward the active region due to the injection of hot carriers through defective states.

A similar analysis in more extreme conditions was carried out by De Santi et al. on MQW LEDs on sapphire [107]. The increase in reverse current during stress and in reverse EL intensity was confirmed even at higher reverse voltages, as was their correlation (see Fig. 2.18). They analyzed also the spatial distribution of the EL signal, which originates from localized conductive paths ("hot spots"). A novelty element is the fact that the number and intensity of "hot spots" increase over stress time (see the inset in Fig. 2.18) and that the failure point (which has a melted appearance) usually corresponds to the peak reverse EL position. This result suggests that catastrophic breakdown occurs due to the high-power dissipation under strong reverse voltage, driven by the increase in the current flowing in a localized region caused by generation and/or percolation of conductive paths created by the electric field.

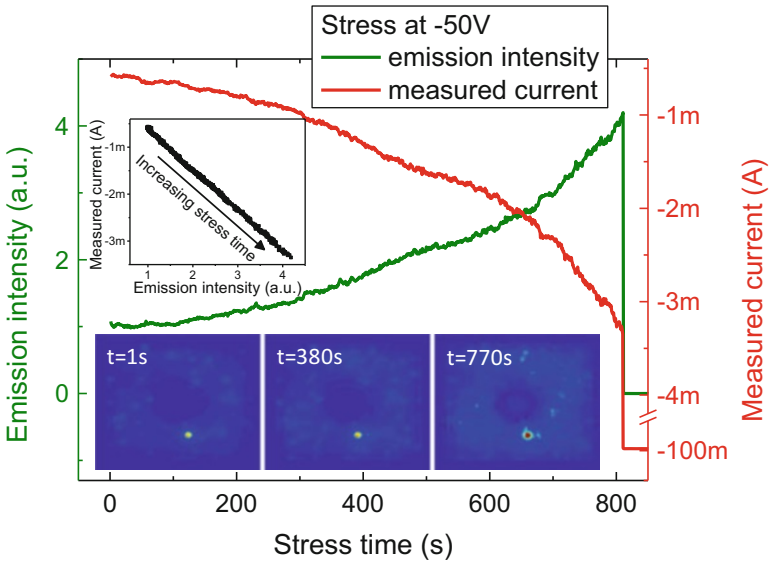


**Fig. 2.18** Increase in leakage current and corresponding reverse-bias electroluminescence during stress test at high negative voltage. Insets show the correlation of the two quantities and the spatially resolved reverse electroluminescence maps at three different aging points

To confirm this hypothesis, they tested several devices at various stress voltages. Experimental results show that the time to failure is Weibull distributed (see Fig. 2.19), suggesting that GaN in deep depletion may behave as a dielectric and be affected by time-dependent dielectric breakdown (TDDB). Time-dependent dielectric breakdown is a time-dependent failure mechanism commonly found in insulating materials and consists in the generation/percolation of conductive paths through field-induced defects shunting the dielectric layer [108–110]. The detected exponential dependence of the failure time on stress voltage (see inset of Fig. 2.19) is a second common signature of TDDB. The fact that GaN itself can be affected by TDDB is an important result for a more clear understanding of the failure mechanism of electronic and optoelectronic devices under high electric fields [111–113].

## 2.9 Conclusions

In summary, the high reliability of GaN-based optoelectronic devices is one of the reasons of their high diffusion in the market of light-emitting devices. Thanks to several improvements in growth techniques and structure, commercial products are almost entirely free from some of the early degradation modes, such as electromigration and device cracking, and even contact robustness is strongly improved.

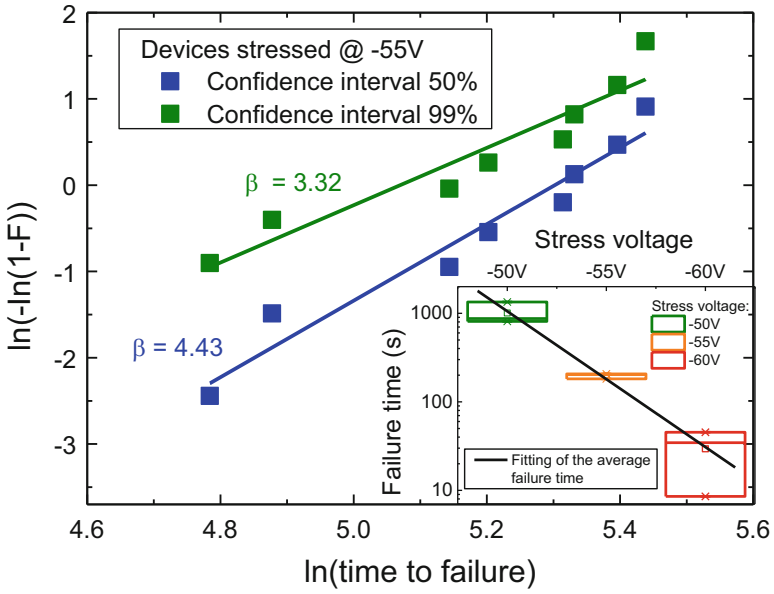


**Fig. 2.19** Weibull plot of the distribution of eight devices stressed under high reverse bias and good agreement with the Weibull distribution. Inset: exponential dependence of the time to failure upon stress voltage

At the state of the art, the most critical aspect to be addressed is the generation of defects during the lifetime. They may lead to premature failure due to short circuiting of the active region, and even a moderate increase in their concentration can strongly affect the output optical power, enhancing the non-radiative recombination. To reach an even higher robustness and performance level, a lower defect density and defect generation rate is a mandatory task, and a more accurate analysis of the causes, impact, and improvements regarding the SRH recombination is required.

Out of the total number of failed luminaires in real applications, a large amount of devices exhibit the typical signatures of failure related to ESD or EOS. Even though the reliability at device level was strongly improved, an important role is played by electrical driver structure, mechanical design, and installation conditions. An analysis and careful planning at system level are therefore required to prevent early failures.

Finally, the very good robustness and performances of light-emitting devices enable creative and advanced solutions, such as AC-driven LEDs and new applications to the automotive field. Each of these is expected to create additional open reliability issues, ranging from the stability under reverse bias to operation at very high temperature and power density.

## References


1. H. Amano, M. Kito, K. Hiramatsu, I. Akasaki, P-type conduction in mg-doped GaN treated with low-energy electron beam irradiation (LEEBI). Jpn. J. Appl. Phys. **28**., no. Part 2(12), L2112–L2114 (1989). doi:10.1143/JJAP.28.L2112
2. X. Li, J.J. Coleman, Time-dependent study of low energy electron beam irradiation of Mg-doped GaN grown by metalorganic chemical vapor deposition. Appl. Phys. Lett. **69** (11), 1605 (1996). doi:10.1063/1.117045
3. A. Sedhain, J. Li, J.Y. Lin, H.X. Jiang, Nature of deep center emissions in GaN. Appl. Phys. Lett. **96**(15), 5–8 (2010). doi:10.1063/1.3389497
4. D.O. Demchenko, I.C. Diallo, M.A. Reshchikov, Yellow luminescence of gallium nitride generated by carbon defect complexes. Phys. Rev. Lett. **110**(8), 1–5 (2013). doi:10.1103/PhysRevLett.110.087404
5. M. La Grassa, M. Meneghini, C. De Santi, M. Mandurrino, M. Goano, F. Bertazzi, R. Zeisel, B. Galler, G. Meneghesso, E. Zanoni, Ageing of InGaN-based LEDs: effects on internal quantum efficiency and role of defects. Microelectron. Reliab. **55**(9), 1775–1778 (2015). doi:10.1016/j.microrel.2015.06.103
6. D. Schiavon, M. Binder, M. Peter, B. Galler, P. Drechsel, F. Scholz, Wavelength-dependent determination of the recombination rate coefficients in single-quantum-well GaInN/GaN light emitting diodes. Phys. Status Solidi B **250**(2), 283–290 (2013). doi:10.1002/pssb.201248286
7. D.V. Lang, Deep-level transient spectroscopy: a new method to characterize traps in semiconductors. J. Appl. Phys. **45**(7), 3023–3032 (1974)
8. M. Buffolo, C. De Santi, M. Meneghini, D. Rigon, G. Meneghesso, E. Zanoni, Long-term degradation mechanisms of mid-power LEDs for lighting applications. Microelectron. Reliab. **55**(9), 1754–1758 (2015). doi:10.1016/j.microrel.2015.06.098
9. Y. Xi, E.F. Schubert, Junction-temperature measurement in GaN ultraviolet light-emitting diodes using diode forward voltage method. Appl. Phys. Lett. **85**(12), 2163–2165 (2004). doi:10.1063/1.1795351
10. M. Auf der Maur, B. Galler, I. Pietzonka, M. Strassburg, H. Lugauer, A. Di Carlo, Trap-assisted tunneling in InGaN/GaN single-quantum-well light-emitting diodes. Appl. Phys. Lett. **105**(13), 133504 (2014). doi:10.1063/1.4896970
11. M. Mandurrino, G. Verzellesi, M. Goano, M. Vallone, F. Bertazzi, G. Ghione, M. Meneghini, G. Meneghesso, E. Zanoni, Physics-based modeling and experimental implications of trap-assisted tunneling in InGaN/GaN light-emitting diodes. Phys. Status Solidi **212**(5), 947–953 (2015). doi:10.1002/pssa.201431743
12. K. Orita, M. Meneghini, H. Ohno, N. Trivellin, N. Ikedo, S. Takigawa, M. Yuri, T. Tanaka, E. Zanoni, G. Meneghesso, Analysis of diffusion-related gradual degradation of InGaN-based laser diodes. IEEE J. Quantum Electron. **48**(9), 1169–1176 (2012). doi:10.1109/JQE.2012.2203795
13. C. De Santi, M. Meneghini, D. Gachet, G. Mura, M. Vanzi, G. Meneghesso, E. Zanoni, Nanoscale investigation of degradation and wavelength fluctuations in InGaN-based green laser diodes. IEEE Trans. Nanotechnol. **15**(2), 274–280 (2016). doi:10.1109/TNANO.2016.2520833
14. P. Kamyczek, E. Placzek-Popko, V. Kolkovsky, S. Grzanka, R. Czernecki, A deep acceptor defect responsible for the yellow luminescence in GaN and AlGaN. J. Appl. Phys. **111**, 113105 (2012). doi:10.1063/1.4725484
15. T. Ogino, M. Aoki, Mechanism of yellow luminescence in GaN. Jpn. J. Appl. Phys. **19**(12), 2395–2405 (1980). doi:10.1063/1.115098
16. J.L. Lyons, a. Janotti, C.G. Van de Walle, Carbon impurities and the yellow luminescence in GaN. Appl. Phys. Lett. **97**(15), 152108 (2010). doi:10.1063/1.3492841

17. J.L. Lyons, a. Janotti, C.G. Van de Walle, Effects of carbon on the electrical and optical properties of InN, GaN, and AlN. Phys. Rev. B **89**(3), 035204 (2014). doi:10.1103/PhysRevB.89.035204
18. J. Neugebauer, C.G. Van de Walle, Gallium vacancies and the yellow luminescence in GaN. Appl. Phys. Lett. **69**(4), 503–505 (1996). doi:10.1063/1.117767
19. C. De Santi, M. Meneghini, G. Meneghesso, E. Zanoni, Degradation of InGaN laser diodes caused by temperature- and current-driven diffusion processes. Microelectron. Reliab. **64**, 623–626 (2016). doi:10.1016/j.microrel.2016.07.118
20. C.H. Seager, S.M. Myers, A.F. Wright, D.D. Koleske, A.A. Allerman, Drift, diffusion, and trapping of hydrogen in p-type GaN. J. Appl. Phys. **92**(12), 7246–7252 (2002). doi:10.1063/1.1520719
21. Y.S. Puzyrev, T. Roy, M. Beck, B.R. Tuttle, R.D. Schrimpf, D.M. Fleetwood, S.T. Pantelides, Dehydrogenation of defects and hot-electron degradation in GaN high-electron-mobility transistors. J. Appl. Phys. **109**(3), 034501 (2011). doi:10.1063/1.3524185
22. H. Nykänen, S. Suihkonen, L. Kilanski, M. Sopanen, F. Tuomisto, Low energy electron beam induced vacancy activation in GaN. Appl. Phys. Lett. **100**(12), 122105 (2012). doi:10.1063/1.3696047
23. S.J. Pearton, C.R. Abernathy, C.B. Vartuli, J.D. Mackenzie, R.J. Shul, R.G. Wilson, J.M. Zavada, Hydrogen incorporation in GaN, AlN, and InN during $Cl_2/CH_4/H_2$/Ar ECR plasma etching. Electron. Lett. **31**(10), 836–837 (1995). doi:10.1049/el:19950558
24. Z. Benzarti, I. Halidou, Z. Bougrioua, T. Boufaden, B. El Jani, Magnesium diffusion profile in GaN grown by MOVPE. J. Cryst. Growth **310**(14), 3274–3277 (2008). doi:10.1016/j.jcrysgro.2008.04.008
25. C.J. Pan, G.C. Chi, The doping of GaN with mg diffusion. Solid State Electron. **43**(3), 621–623 (1999). doi:10.1016/S0038-1101(98)00289-5
26. H. Xing, D.S. Green, H. Yu, T. Mates, P. Kozodoy, S. Keller, S.P. Denbaars, U.K. Mishra, Memory effect and redistribution of mg into sequentially regrown GaN layer by metalorganic chemical vapor deposition. Jpn. J. Appl. Phys. **42**(1), 50–53 (2003). doi:10.1143/JJAP.42.50
27. J.C. Zolper, S.J. Pearton, R.G. Wilson, R.A. Stall, Implant activation and redistribution of dopants in GaN. Proc. 11th Int. Conf. Ion Implant. Technol. 705–708 (1996). doi:10.1109/IIT.1996.586515
28. K. Harafuji, K. Kawamura, Magnesium diffusion at dislocation in wurtzite-type GaN crystal. Jpn. J. Appl. Phys. **44**(9A), 6495–6504 (2005). doi:10.1143/JJAP.44.6495
29. K. Harafuji, T. Tsuchiya, K. Kawamura, Magnesium diffusion in wurtzite-type GaN crystal. Jpn. J. Appl. Phys. **0**(7), 2240–2243 (2003). doi:10.1002/pssc.200303298
30. K. Harafuji, T. Tsuchiya, K. Kawamura, Molecular dynamics of magnesium diffusion in Wurtzite-type GaN crystal. Jpn. J. Appl. Phys. **43**(2), 522–531 (2004). doi:10.1143/JJAP.43.522
31. S.M. Myers, A.F. Wright, G.A. Petersen, C.H. Seager, W.R. Wampler, M.H. Crawford, J. Han, Equilibrium state of hydrogen in gallium nitride: theory and experiment. J. Appl. Phys. **88**(8), 4676–4687 (2000). doi:10.1063/1.1309123
32. S.M. Myers, A.F. Wright, Theoretical description of H behavior in GaN p-n junctions. J. Appl. Phys. **90**(11), 5612–5622 (2001). doi:10.1063/1.1413950
33. W.R. Wampler, S.M. Myers, Hydrogen release from magnesium-doped GaN with clean ordered surfaces. J. Appl. Phys. **94**(9), 5682–5687 (2003). doi:10.1063/1.1616986
34. C.G. Van de Walle, N.M. Johnson, in *Semiconductors and Semimetals*, vol 57, ed. by J.I. Pankove, T.D. Moustakas. Hydrogen in III–V nitrides (Academic, Boston, 1999), pp. 157–184
35. M. Meneghini, S. Podda, A. Morelli, R. Pintus, L. Trevisanello, G. Meneghesso, M. Vanzi, E. Zanoni, High brightness GaN LEDs degradation during dc and pulsed stress. Microelectron. Reliab. **46**(9–11), 1720–1724 (2006). doi:10.1016/j.microrel.2006.07.050
36. M. Meneghini, L. Trevisanello, U. Zehnder, T. Zahner, U. Strauss, G. Meneghesso, E. Zanoni, High-temperature degradation of GaN LEDs related to passivation. IEEE Trans. Electron Devices **53**(12), 2981–2987 (2006). doi:10.1109/TED.2006.885544

37. M. Meneghini, L.-R. Trevisanello, U. Zehnder, G. Meneghesso, E. Zanoni, Reversible degradation of Ohmic contacts on p-GaN for application in high-brightness LEDs. IEEE Trans. Electron Devices **54**(12), 3245–3251 (2007). doi:10.1109/TED.2007.908900
38. H. Omiya, F.A. Ponce, H. Marui, S. Tanaka, T. Mukai, Atomic arrangement at the Au/p-GaN interface in low-resistance contacts. Appl. Phys. Lett. **85**(25), 6143 (2004). doi:10.1063/1.1840105
39. L. Stafford, L.F. Voss, S.J. Pearton, H.T. Wang, F. Ren, Improved long-term thermal stability of InGaN/GaN multiple quantum well light-emitting diodes using $TiB_2$- and Ir-based p-Ohmic contacts. Appl. Phys. Lett. **90**(24), 242103 (2007). doi:10.1063/1.2748306
40. D.L. Barton, J. Zeller, B.S. Phillips, Pei-Chih Chiu, S. Askar, Dong-Seung Lee, M. Osinski, K.J. Malloy, in *33rd IEEE International Reliability Physics Symposium*. Degradation of blue AlGaN/InGaN/GaN LEDs subjected to high current pulses (1995), pp. 191–199, doi:10.1109/RELPHY.1995.513674
41. M. Osiński, J. Zeller, P.-C. Chiu, B. Scott Phillips, D.L. Barton, AlGaN/InGaN/GaN blue light emitting diode degradation under pulsed current stress. Appl. Phys. Lett. **69**(7), 898 (1996). doi:10.1063/1.116936
42. H. Kim, H. Yang, C. Huh, S.-W. Kim, S.-J. Park, H. Hwang, Electromigration-induced failure of GaN multi-quantum well light emitting diode. Electron. Lett. **36**(10), 908 (2000). doi:10.1049/el:20000657
43. C.-Y. Hsu, W.-H. Lan, Y.S. Wu, Effect of thermal annealing of Ni/Au ohmic contact on the leakage current of GaN based light emitting diodes. Appl. Phys. Lett. **83**(12), 2447 (2003). doi:10.1063/1.1601306
44. L. Liu, L. Yin, D. Teng, J. Zhang, X. Ma, G. Wang, An explanation for catastrophic failures of GaN-based vertical structure LEDs subjected to thermoelectric stressing. J. Phys. D **48**(30), 305102 (2015). doi:10.1088/0022-3727/48/30/305102
45. A. Krost, A. Dadgar, GaN-based optoelectronics on silicon substrates. Mater. Sci. Eng. B **93**(1–3), 77–84 (2002). doi:10.1016/S0921-5107(02)00043-0
46. A. Sarua, S. Rajasingam, M. Kuball, C. Younes, B. Yavich, W.N. Wang, High temperature annealing of AlGaN: stress and composition changes. Phys. Status Solidi **1**, 568–571 (2003). doi:10.1002/pssc.200390115
47. D.L. Barton, M. Osinski, P. Perlin, C.J. Helms, N.H. Berg, in *1997 I.E. International Reliability Physics Symposium Proceedings. 35th Annual* . Life tests and failure mechanisms of GaN/AlGaN/InGaN light emitting diodes (1997), pp. 276–281. doi:10.1109/RELPHY.1997.584273
48. N.P. Kobayashi, J.T. Kobayashi, P.D. Dapkus, W.-J. Choi, A.E. Bond, X. Zhang, D.H. Rich, GaN growth on Si(111) substrate using oxidized AlAs as an intermediate layer. Appl. Phys. Lett. **71**(24), 3569 (1997). doi:10.1063/1.120394
49. A. Strittmatter, A. Krost, M. Straßburg, V. Türck, D. Bimberg, J. Bläsing, J. Christen, Low-pressure metal organic chemical vapor deposition of GaN on silicon(111) substrates using an AlAs nucleation layer. Appl. Phys. Lett. **74**(9), 1242 (1999). doi:10.1063/1.123512
50. H. Amano, N. Sawaki, I. Akasaki, Y. Toyoda, Metalorganic vapor phase epitaxial growth of a high quality GaN film using an AlN buffer layer. Appl. Phys. Lett. **48**(5), 353 (1986). doi:10.1063/1.96549
51. H. Lahrèche, P. Vennéguès, O. Tottereau, M. Laügt, P. Lorenzini, M. Leroux, B. Beaumont, P. Gibart, Optimisation of AlN and GaN growth by metalorganic vapour-phase epitaxy (MOVPE) on Si (111). J. Cryst. Growth **217**(1–2), 13–25 (2000). doi:10.1016/S0022-0248(00)00478-4
52. A.T. Schremer, J.A. Smart, Y. Wang, O. Ambacher, N.C. MacDonald, J.R. Shealy, High electron mobility AlGaN/GaN heterostructure on (111) Si. Appl. Phys. Lett. **76**(6), 736 (2000). doi:10.1063/1.125878
53. H. Amano, M. Iwaya, N. Hayashi, T. Kashima, S. Nitta, C. Wetzel, I. Akasaki, Control of dislocations and stress in AlGaN on sapphire using a low temperature interlayer. Phys. Status

Solidi **216**(1), 683–689 (1999). doi:10.1002/(SICI)1521-3951(199911)216:1<683::AID-PSSB683>3.0.CO;2-4
54. A. Dadgar, J. Bläsing, A. Diez, A. Alam, M. Heuken, A. Krost, Metalorganic chemical vapor phase epitaxy of crack-free GaN on Si (111) exceeding 1 μm in thickness. Jpn. J. Appl. Phys. **39**., no. Part 2(11B), L1183–L1185 (2000). doi:10.1143/JJAP.39.L1183
55. A. Reiher, J. Bläsing, A. Dadgar, A. Diez, A. Krost, Efficient stress relief in GaN heteroepitaxy on Si(111) using low-temperature AlN interlayers. J. Cryst. Growth **248**, 563–567 (2003). doi:10.1016/S0022-0248(02)01880-8
56. K. Cheng, M. Leys, S. Degroote, M. Germain, G. Borghs, High quality GaN grown on silicon (111) using a $Si_xN_y$ interlayer by metal-organic vapor phase epitaxy. Appl. Phys. Lett. **92**(19), 192111 (2008). doi:10.1063/1.2928224
57. H. Marchand, L. Zhao, N. Zhang, B. Moran, R. Coffie, U.K. Mishra, J.S. Speck, S.P. DenBaars, J.A. Freitas, Metalorganic chemical vapor deposition of GaN on Si(111): stress control and application to field-effect transistors. J. Appl. Phys. **89**(12), 7846 (2001). doi:10.1063/1.1372160
58. K. Cheng, M. Leys, S. Degroote, B. Van Daele, S. Boeykens, J. Derluyn, M. Germain, G. Van Tendeloo, J. Engelen, G. Borghs, Flat GaN epitaxial layers grown on Si(111) by metalorganic vapor phase epitaxy using step-graded AlGaN intermediate layers. J. Electron. Mater. **35**(4), 592–598 (2006). doi:10.1007/s11664-006-0105-1
59. J. Lee, Y. Tak, J.-Y. Kim, H.-G. Hong, S. Chae, B. Min, H. Jeong, J. Yoo, J.-R. Kim, Y. Park, Growth of high-quality InGaN/GaN LED structures on (111) Si substrates with internal quantum efficiency exceeding 50%. J. Cryst. Growth **315**(1), 263–266 (2011). doi:10.1016/j.jcrysgro.2010.08.006
60. P. Saengkaew, A. Dadgar, J. Blaesing, T. Hempel, P. Veit, J. Christen, A. Krost, Low-temperature/high-temperature AlN superlattice buffer layers for high-quality $Al_xGa_{1-x}N$ on Si (111). J. Cryst. Growth **311**(14), 3742–3748 (2009). doi:10.1016/j.jcrysgro.2009.04.038
61. S.-H. Jang, C.-R. Lee, High-quality GaN/Si(111) epitaxial layers grown with various $Al_{0.3}Ga_{0.7}N$/GaN superlattices as intermediate layer by MOCVD. J. Cryst. Growth **253** (1–4), 64–70 (2003). doi:10.1016/S0022-0248(03)01015-7
62. E. Feltin, B. Beaumont, M. Laugt, P. de Mierry, P. Vennegues, M. Leroux, P. Gibart, Crack-free thick GaN layers on silicon (111) by metalorganic vapor phase epitaxy. Phys. Status Solidi **188**(2), 531–535 (2001). doi:10.1002/1521-396X(200112)188:2<531::AID-PSSA531>3.0.CO;2-V
63. L. Zhang, W.-S. Tan, S. Westwater, A. Pujol, A. Pinos, S. Mezouari, K. Stribley, J. Whiteman, J. Shannon, K. Strickland, High brightness GaN-on-Si based blue LEDs grown on 150 mm Si substrates using thin buffer layer technology. IEEE J. Electron Devices Soc. **3**(6), 457–462 (2015). doi:10.1109/JEDS.2015.2463738
64. Y. Honda, Y. Kuroiwa, M. Yamaguchi, N. Sawaki, Growth of GaN free from cracks on a (111)Si substrate by selective metalorganic vapor-phase epitaxy. Appl. Phys. Lett. **80**(2), 222 (2002). doi:10.1063/1.1432764
65. J. Xu, L. Chen, L. Yu, H. Liang, B.L. Zhang, K.M. Lau, Temperature dependence of cathodoluminescence spectra and stress analysis of a GaN layer grown on a mesa structured Si substrate. J. Appl. Phys. **102**(10), 104508 (2007). doi:10.1063/1.2817614
66. S.-J. Lee, G.H. Bak, S.-R. Jeon, S.H. Lee, S.-M. Kim, S.H. Jung, C.-R. Lee, I.-H. Lee, S.-J. Leem, J.H. Baek, Epitaxial growth of crack-free GaN on patterned Si(111) substrate. Jpn. J. Appl. Phys. **47**(4), 3070–3073 (2008). doi:10.1143/JJAP.47.3070
67. T. Boufaden, A. Matoussi, S. Guermazi, S. Juillaguet, A. Toureille, Y. Mlik, B. El Jani, Optical properties of GaN grown on porous silicon substrate. Phys. Status Solidi **201**(3), 582–587 (2004). doi:10.1002/pssa.200306740
68. K. Cheng, S. Degroote, M. Leys, B. Van Daele, M. Germain, G. Van Tendeloo, G. Borghs, Single crystalline GaN grown on porous Si(111) by MOVPE. Phys. Status Solidi **4**(6), 1908–1912 (2007). doi:10.1002/pssc.200674316

69. H. Ishikawa, K. Shimanaka, F. Tokura, Y. Hayashi, Y. Hara, M. Nakanishi, MOCVD growth of GaN on porous silicon substrates. J. Cryst. Growth **310**(23), 4900–4903 (2008). doi:10.1016/j.jcrysgro.2008.08.030
70. A.H. Blake, D. Caselli, C. Durot, J. Mueller, E. Parra, J. Gilgen, A. Boley, D.J. Smith, I.S.T. Tsong, J.C. Roberts, E. Piner, K. Linthicum, J.W. Cook, D.D. Koleske, M.H. Crawford, A.J. Fischer, InGaN/GaN multiple-quantum-well light-emitting diodes grown on Si(111) substrates with $ZrB_2$(0001) buffer layers. J. Appl. Phys. **111**(3), 033107 (2012). doi:10.1063/1.3684557
71. G. Meneghesso, A. Chini, A. Maschietto, E. Zanoni, P. Malberti, M. Ciappa, in *Electrical Overstress/Electrostatic Discharge Symposium, 2001. EOS/ESD '01* . Electrostatic discharge and electrical overstress on GaN/InGaN light emitting diodes (2001), pp. 247–252
72. S.-M. Kim, H.S. Oh, J.H. Baek, T.-Y. Park, G.Y. Jung, Negative-voltage electrostatic discharge characteristics of blue light-emitting diodes using an extended n-electrode onto plasma treated p-GaN. Appl. Phys. Express **4**(7), 072102 (2011). doi:10.1143/APEX.4.072102
73. M. Meneghini, A. Tazzoli, G. Mura, G. Meneghesso, E. Zanoni, A review on the physical mechanisms that limit the reliability of GaN-based LEDs. IEEE Trans. Electron Devices **57** (1), 108–118 (2010). doi:10.1109/TED.2009.2033649
74. M. Meneghini, A. Tazzoli, E. Ranzato, N. Trivellin, G. Meneghesso, E. Zanoni, M. Pavesi, M. Manfredi, R. Butendeich, U. Zehnder, B. Hahn, A study of the failure of GaN-based LEDs submitted to reverse-bias stress and ESD events. 2010 I.E. Int. Reliab. Phys. Symp. 522–527 (2010). doi:10.1109/IRPS.2010.5488776
75. Y.K. Su, S.J. Chang, S.C. Wei, ESD engineering of nitride-based LEDs. IEEE Trans. Device Mater. Reliab. **5**(2), 277–281 (2005). doi:10.1109/TDMR.2005.847197
76. C.M. Tsai, J.K. Sheu, P.T. Wang, W.C. Lai, S.C. Shei, S.J. Chang, C.H. Kuo, C.W. Kuo, Y.K. Su, High efficiency and improved ESD characteristics of GaN-based LEDs with naturally textured surface grown by MOCVD. IEEE Photon. Technol. Lett. **18**(11), 1213–1215 (2006). doi:10.1109/LPT.2006.875063
77. S. Kitamura, K. Hiramatsu, N. Sawaki, Fabrication of GaN hexagonal pyramids on dot-patterned GaN/sapphire substrates via selective metalorganic vapor phase epitaxy. Jpn. J. Appl. Phys. **34**., no. Part 2(9B), L1184–L1186 (1995). doi:10.1143/JJAP.34.L1184
78. D.I. Florescu, S.M. Ting, J.C. Ramer, D.S. Lee, V.N. Merai, A. Parkeh, D. Lu, E.A. Armour, L. Chernyak, Investigation of V-defects and embedded inclusions in InGaN/GaN multiple quantum wells grown by metalorganic chemical vapor deposition on (0001) sapphire. Appl. Phys. Lett. **83**(1), 33 (2003). doi:10.1063/1.1588370
79. S.M. Ting, J.C. Ramer, D.I. Florescu, V.N. Merai, B.E. Albert, A. Parekh, D.S. Lee, D. Lu, D.V. Christini, L. Liu, E.A. Armour, Morphological evolution of InGaN/GaN quantum-well heterostructures grown by metalorganic chemical vapor deposition. J. Appl. Phys. **94**(3), 1461 (2003). doi:10.1063/1.1586972
80. P. Li, H. Li, Y. Zhao, J. Kang, Z. Li, Z. Liu, X. Yi, J. Li, G. Wang, Excellent ESD resistance property of InGaN LEDs with enhanced internal capacitance. IEEE Photon. Technol. Lett. **27** (19), 2004–2006 (2015). doi:10.1109/LPT.2015.2448418
81. S.-K. Jeon, J.-G. Lee, E.-H. Park, J. Jang, J.-G. Lim, S.-K. Kim, J.-S. Park, The effect of the internal capacitance of InGaN-light emitting diode on the electrostatic discharge properties. Appl. Phys. Lett. **94**(13), 131106 (2009). doi:10.1063/1.3114974
82. C. Jia, C. Zhong, T. Yu, Z. Wang, Y. Tong, G. Zhang, Improvement of electrostatic discharge characteristics of InGaN/GaN MQWs light-emitting diodes by inserting an $n^+$-InGaN electron injection layer and a p-InGaN/GaN hole injection layer. Semicond. Sci. Technol. **27**(6), 065008 (2012). doi:10.1088/0268-1242/27/6/065008
83. M. Meneghini, A. Tazzoli, R. Butendeich, B. Hahn, G. Meneghesso, E. Zanoni, Soft and hard failures of InGaN-based LEDs submitted to electrostatic discharge testing. IEEE Electron Device Lett. **31**(6), 579–581 (2010). doi:10.1109/LED.2010.2045874

84. M. Dal Lago, M. Meneghini, C. De Santi, M. Barbato, N. Trivellin, G. Meneghesso, E. Zanoni, ESD on GaN-based LEDs: an analysis based on dynamic electroluminescence measurements and current waveforms. Microelectron. Reliab. **54**(9–10), 2138–2141 (2014). doi:10.1016/j.microrel.2014.07.122
85. C.-H. Chen, S.-J. Chang, Y.-K. Su, High electrostatic discharge protection of InGaN/GaN MQW LEDs by using GaN Schottky diodes. Phys. Status Solidi **200**(1), 91–94 (2003). doi:10.1002/pssa.200303496
86. T.C. Wen, S.J. Chang, Y.K. Su, L.W. Wu, C.H. Kuo, Y.P. Hsu, W.C. Lai, J.K. Sheu, Improved ESD reliability by using a modulation doped $Al_{0.12}Ga_{0.88}N$/GaN superlattice in nitride-based LED. Int. Semicond. Device Res. Symp. 2003 77–78 (2003). doi:10.1109/ISDRS.2003.1272004.
87. Y.J. Liu, C.H. Yen, L.Y. Chen, T.H. Tsai, T.Y. Tsai, W.C. Liu, On a GaN-based light-emitting diode with a p-GaN/i-InGaN superlattice structure. IEEE Electron Device Lett. **30** (11), 1149–1151 (2009). doi:10.1109/LED.2009.2030140
88. S.-C. Shei, J.-K. Sheu, C.-F. Shen, Improved reliability and ESD characteristics of Flip-Chip GaN-based LEDs with internal inverse-parallel protection diodes. IEEE Electron Device Lett. **28**(5), 346–349 (2007). doi:10.1109/LED.2007.895428
89. H.H. Jeong, S.Y. Lee, J.-H. Bae, K.K. Choi, J.-O. Song, S.J. Son, Y.-H. Lee, T.-Y. Seong, Improved electrostatic discharge protection in GaN-based vertical light-emitting diodes by an internal diode. IEEE Photon. Technol. Lett. **23**(7), 423–425 (2011). doi:10.1109/LPT.2011.2106204
90. C.-H. Jang, J.K. Sheu, C.M. Tsai, S.C. Shei, W.C. Lai, S.J. Chang, Effect of thickness of the p-AlGaN electron blocking layer on the improvement of ESD characteristics in GaN-based LEDs. IEEE Photon. Technol. Lett. **20**(13), 1142–1144 (2008). doi:10.1109/LPT.2008.924886
91. T.Y. Park, M.S. Oh, S.J. Park, Improvement of electrostatic discharge characteristics and optical properties of GaN-based light-emitting diodes. IEEE Electron Device Lett. **30**(9), 937–939 (2009). doi:10.1109/LED.2009.2025783
92. P.C. Tsai, W.R. Chen, Y.K. Su, Enhanced ESD properties of GaN-based light-emitting diodes with various MOS capacitor designs. Superlattice. Microst. **48**(1), 23–30 (2010). doi:10.1016/j.spmi.2010.04.006
93. S.L. Chen, Enhanced electrostatic discharge reliability in GaN-based light-emitting diodes by the electrode engineering. J. Disp. Technol. **10**(10), 807–813 (2014). doi:10.1109/JDT.2014.2321460
94. X.-H. Huang, J.-P. Liu, Y.-M. Fan, J.-J. Kong, H. Yang, H.-B. Wang, Improving InGaN-LED performance by optimizing the patterned sapphire substrate shape. Chinese Phys. B **21**(3), 037105 (2012). doi:10.1088/1674-1056/21/3/037105
95. K.H. Lee, Y.-T. Moon, S.K. Oh, J.S. Kwak, High efficiency and ESD of GaN-based LEDs with patterned ion-damaged current blocking layer. IEEE Photon. Technol. Lett. **27**(2), 149–152 (2015). doi:10.1109/LPT.2014.2362982
96. M. Dal Lago, M. Meneghini, N. Trivellin, G. Mura, M. Vanzi, G. Meneghesso, E. Zanoni, 'Hot-plugging' of LED modules: electrical characterization and device degradation. Microelectron. Reliab. **53**(9–11), 1524–1528 (2013). doi:10.1016/j.microrel.2013.07.054
97. M. Meneghini, C. De Santi, M. Buffolo, A. Munaretto, G. Meneghesso, E. Zanoni, in *2015 12th China International Forum on Solid State Lighting (SSLCHINA)*. Towards high reliability GaN LEDs: understanding the physical origin of gradual and catastrophic failure (2015), pp. 63–66. doi:10.1109/SSLCHINA.2015.7360690
98. H.-H. Yen, W.-Y. Yeh, H.-C. Kuo, GaN alternating current light-emitting device. Phys. Status Solidi **204**(6), 2077–2081 (2007). doi:10.1002/pssa.200674766
99. J. Cho, J. Jung, J.H. Chae, H. Kim, H. Kim, J.W. Lee, S. Yoon, C. Sone, T. Jang, Y. Park, E. Yoon, Alternating-current light emitting diodes with a diode bridge circuitry. Jpn. J. Appl. Phys. **46**(48), L1194–L1196 (2007). doi:10.1143/JJAP.46.L1194

100. H.-H. Yen, H.-C. Kuo, W.-Y. Yeh, Characteristics of single-chip GaN-based alternating current light-emitting diode. Jpn. J. Appl. Phys. **47**(12), 8808–8810 (2008). doi:10.1143/JJAP.47.8808
101. G.A. Onushkin, Y.-J. Lee, J.-J. Yang, H.-K. Kim, J.-K. Son, G.-H. Park, Y. Park, Efficient alternating current operated white light-emitting diode chip. IEEE Photon. Technol. Lett. **21** (1), 33–35 (2009). doi:10.1109/LPT.2008.2008204
102. H.H. Yen, H.C. Kuo, W.Y. Yeh, Particular failure mechanism of GaN-based alternating current light-emitting diode induced by $GaO_x$ oxidation. IEEE Photon. Technol. Lett. **22**(15), 1168–1170 (2010). doi:10.1109/LPT.2010.2051424
103. W.Y. Yeh, H.H. Yen, Y.J. Chan, The development of monolithic alternating current light-emitting diode. SPIE OPTO 793910–793912 (2011). doi:10.1117/12.873668
104. Y. Gao, H. Zhang, X. Guo, F. Cao, J. Yu, A. Chen, N. Zou, Method to design alternating current light-emitting diodes luminous flux. Opt. Quant. Electron. **47**(12), 3715–3727 (2015). doi:10.1007/s11082-015-0241-z
105. H. Chen, B. Yun Huang, Y. Cheng Chu, Degradation mechanisms in GaN light-emitting diodes undergoing reverse-bias operations in water vapor. Appl. Phys. Lett. **103**(17), 8–11 (2013). doi:10.1063/1.4826254
106. M. Meneghini, U. Zehnder, B. Hahn, G. Meneghesso, E. Zanoni, Degradation of high-brightness green LEDs submitted to reverse electrical stress. IEEE Electron Device Lett. **30**(10), 1051–1053 (2009). doi:10.1109/LED.2009.2029129
107. C. De Santi, M. Meneghini, M. Buffolo, G. Meneghesso, E. Zanoni, Experimental demonstration of time-dependent breakdown in GaN-based light emitting diodes. IEEE Electron Device Lett. **37**(5), 611–614 (2016). doi:10.1109/LED.2016.2543805
108. R. Degraeve, G. Groeseneken, R. Bellens, J.L. Ogier, M. Depas, P.J. Roussel, H.E. Maes, New insights in the relation between electron trap generation and the statistical properties of oxide breakdown. IEEE Trans. Electron Devices **45**(4), 904–911 (1998). doi:10.1109/16.662800
109. J.H. Stathis, Percolation models for gate oxide breakdown. J. Appl. Phys. **86**(10), 5757 (1999). doi:10.1063/1.371590
110. T. Kauerauf, R. Degraeve, M.B. Zahid, M. Cho, B. Kaczer, P. Roussel, G. Groeseneken, H. Maes, S. De Gendt, Abrupt breakdown in dielectric/metal gate stacks: a potential reliability limitation? IEEE Electron Device Lett. **26**(10), 773–775 (2005). doi:10.1109/LED.2005.856015
111. D. Marcon, T. Kauerauf, F. Medjdoub, J. Das, M. Van Hove, P. Srivastava, K. Cheng, M. Leys, R. Mertens, S. Decoutere, G. Meneghesso, E. Zanoni, G. Borghs, in *2010 International Electron Devices Meeting*. A comprehensive reliability investigation of the voltage-, temperature- and device geometry-dependence of the gate degradation on state-of-the-art GaN-on-Si HEMTs (2010), pp. 20.3.1–20.3.4. doi:10.1109/IEDM.2010.5703398
112. M. Meneghini, O. Hilt, C. Fleury, R. Silvestri, M. Capriotti, G. Strasser, D. Pogany, E. Bahat-Treidel, F. Brunner, A. Knauer, J. Würfl, I. Rossetto, E. Zanoni, G. Meneghesso, S. Dalcanale, Normally-off GaN-HEMTs with p-type gate: off-state degradation, forward gate stress and ESD failure. Microelectron. Reliab. (2015). doi:10.1016/j.microrel.2015.11.026
113. M. Ťapajna, O. Hilt, E. Bahat-Treidel, J. Würfl, J. Kuzmík, Investigation of gate-diode degradation in normally-off p-GaN/AlGaN/GaN high-electron-mobility transistors. Appl. Phys. Lett. **107**(19), 193506 (2015). doi:10.1063/1.4935223

http://www.springer.com/978-3-319-58174-3

Solid State Lighting Reliability Part 2
Components to Systems
van Driel, W.D.; Fan, X.; Zhang, G.Q. (Eds.)
2018, XI, 606 p. 401 illus., 338 illus. in color., Hardcover
ISBN: 978-3-319-58174-3